

**CHARACTERIZATION OF PLASMA SPRAYED SEASHELL
DERIVED HYDROXYAPATITE COATING ON TITANIUM
ALLOY (Ti-6Al-4V ELI)**

M.Tech. Thesis

By

ZUBER ALI SHAH



**DEPARTMENT OF MECHANICAL ENGINEERING
INDIAN INSTITUTE OF TECHNOLOGY INDORE**

MAY 2022

**CHARACTERIZATION OF PLASMA SPRAYED SEASHELL
DERIVED HYDROXYAPATITE COATING ON TITANIUM
ALLOY (Ti-6Al-4V ELI)**

A THESIS

*Submitted in partial fulfillment of the
requirements for the award of the degree*

of

Master of Technology

in

Production and Industrial Engineering

by

Zuber Ali Shah



**DEPARTMENT OF MECHANICAL ENGINEERING
INDIAN INSTITUTE OF TECHNOLOGY INDORE**

MAY 2022



INDIAN INSTITUTE OF TECHNOLOGY INDORE

CANDIDATE'S DECLARATION

I hereby certify that the work which is being presented in the thesis entitled “**CHARACTERIZATION OF PLASMA SPRAYED SEASHELL DERIVED HYDROXYAPATITE COATING ON TITANIUM ALLOY (Ti-6Al-4V ELI)**” in the partial fulfillment of the requirements for the award of the degree of **MASTER OF TECHNOLOGY** and submitted in the **Department of Mechanical Engineering, Indian Institute of Technology Indore**, is an authentic record of my own work carried out during the time period from August 2020 to May 2022 under the supervision of **Dr. Kazi Sabiruddin**, Associate Professor, **Department** of Mechanical Engineering and Indian Institute of Technology (IIT) Indore.

The matter presented in this thesis has not been submitted by me for the award of any other degree of this or any other institute.

Zuber Ali Shah

This is to certify that the above statement made by the candidate is correct to the best of my knowledge.

Dr. Kazi Sabiruddin

Zuber Ali Shah has successfully given her M.Tech. Oral Examination held on **23rd May 2022**.

Signature(s) of Supervisor(s) of M.Tech. thesis
Date: 23/5/22

Convener, DPGC
Date: 02/06/2022

Signature of PSPC Member 1
Dr Ashish Rajak
Date: 02/06/2022

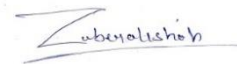
Signature of PSPC Member 2
Dr Apurba K Das
Date:02/06/2022

ACKNOWLEDGEMENTS

My deep gratitude goes first to my supervisor, **Dr. Kazi Sabiruddin**, who expertly guided me throughout my two years of Master of Technology. I was fortunate to have advisors who offered me the constant motivation and productive support that preceded this work to attain this form. I would also like to thank my PSPC members, **Dr. Ashish Rajak** and **Dr. Apurba K Das**, for their continuous input for the advancement of this project.

A very special thanks to **Mr. Shahid Hussain** (Ph.D. scholar), **Mr. Avinandan Khaira** (Ph.D. scholar), and **Mr. Vaibhav Nemane** (Ph.D. scholar) for their moral support and supportive environment for the completion of the project. Thanks also goes to **Mr. Rishabh Gupta**, **Mr. Shubham Birle**, **Ms. Sonali Brahmane**, and my other batch-mates for their moral support throughout this journey.

I cannot end my words without expressing my heartfelt thanks and admiration for my dear parents' blessings and efforts to maintain my morale throughout my project. I would like to offer my heartfelt gratitude to everyone who has assisted me in any way, whether directly or indirectly, during this project.



With Regards,

Dedicated to my parents for their efforts, caring, and blessing

Abstract

Surface coating is the process of modifying the surface of the material to enhance its properties. The investigation of the project is depositing the spray-dried synthesized hydroxyapatite (HA) powder on titanium alloy substrate by using an atmospheric plasma spray process and characterizing the coatings to explore mechanical and microstructural properties. Vickers microhardness and scratch tests are performed to calculate the hardness value and adhesion strength of the coatings, respectively. Ball on disc test on the coatings is conducted to analyze the wear resistance and mass loss. The crystalline phase and roughness of coated samples are analyzed through an X-ray diffractometer (XRD) and stylus profilometer, respectively. A field emission scanning electron microscope (FESEM) is used to characterize the coated samples microstructurally. The XRD graph shows that the stable phase and almost pure hydroxyapatite are obtained at 1000 °C synthesized temperature. The roughness of the coating increases first, and further decreases as the synthesized temperature rises, and minimum roughness is obtained at 1000 °C. It has been noticed as the synthesizing temperature is raised from 700 to 900 °C, the coating hardness increases first, and maximum hardness is reached at 900 °C and then decreases further. The minimum porosity is observed for coating obtained from 1000 °C synthesis temperature HA.

TABLE OF CONTENTS

LIST OF FIGURES

LIST OF TABLES

ACRONYMS

Chapter 1: Introduction.....	1
1.1 Research background	1
1.2 Surface coating.....	1
1.3 Thermal spray.....	2
1.3.1 Flame spray.....	3
1.3.2 Atmospheric plasma spray.....	4
1.3.3 HVOF spray.....	5
1.3.4 Electric arc spray.....	5
1.3.5 Cold spray.....	6
1.3.6 Detonation gun (D- gun).....	7
1.4 Plasma spraying.....	8
1.4.1 Components of plasma spraying.....	10
1.4.2 Process parameters used in plasma spraying.....	10
1.4.3 Requirement of plasma spraying.....	13
Chapter 2: Literature Survey.....	14
2.1 Plasma spray processes for different coating materials.....	14

2.2 Objectives of Research.....	16
Chapter 3: Materials and Method.....	17
3.1 Plasma Spraying.....	17
3.2 The Plasma Spraying System.....	17
3.3 Materials.....	18
3.3.1 Substrate.....	18
3.4.2 Coating Material.....	19
3.5 Substrate Preparation.....	19
3.5.1 Grit Blasting Procedure.....	19
3.5.2 Substrate Cleaning Procedure.....	19
3.6 Characterization of Coatings.....	20
3.6.1 XRD Analysis.....	20
3.6.2 Roughness Measurement.....	21
3.6.3 Mounting, Grinding, and Polishing.....	22
3.6.4 Thickness Measurement.....	23
3.6.5 Microstructural Study of the Coatings.....	24
3.6.6 Porosity Measurement.....	25
3.6.7 Micro Hardness Measurement.....	25
3.6.8 Scratch Analysis.....	26
3.6.9 Wear Analysis.....	27

Chapter 4: Results and Discussion.....	29
4.1 XRD analysis.....	30
4.2 Thickness measurement	30
4.3 Roughness measurement	31
4.4 Porosity measurement.....	32
4.5 Microstructural study of the coatings.....	33
4.1 Top Surface Morphology.....	33
4.2 Cross section Morphology.....	36
4.6 Micro hardness measurement.....	38
4.7 Scratch analysis.....	39
4.7.1. Scratch hardness and fracture toughness.....	39
4.7.2. Coefficient of friction and tractional force.....	40
4.8 Wear analysis.....	43
Chapter 5: Conclusions.....	45
References.....	46

LIST OF FIGURES

Fig. 1.1. Schematic diagram of Powder Flame Spray	3
Fig. 1.2. Schematic diagram of Plasma Spray Process.....	4
Fig. 1.3. Schematic diagram of HVOF Spray.....	5
Fig. 1.4. Schematic diagram of Electric arc spray.....	6
Fig. 1.5. Schematic diagram of cold spray.....	7
Fig. 1.6. Schematic diagram of D Gun.....	8
Fig. 1.7. Setup of plasma spray Process.....	9
Fig. 3.1. Setup of X ray Diffractometer.....	21
Fig. 3.2 Setup of Taylor and Hobson Profilometer.....	22
Fig. 3.3 Setup of High-Speed Cutter.....	22
Fig. 3.4. Setup of Scanning Electron Microscope.....	24
Fig. 3.5. Schematic of Vickers's Hardness test.....	26
Fig. 3.6. Schematic of Ball on Disc Test.....	27
Fig. 4.1. XRD pattern of TCP HA coating and various synthesized temperature.....	30
Fig. 4.2 Thickness value of TCP coating and various temperature synthesized HA coatings.....	31
Fig. 4.3. Roughness value of TCP coating and various temperature synthesized HA coatings.....	32
Fig. 4.4. Variation of Porosity of TCP Coating and various synthesized temperature HA coatings.....	33
Fig. 4.5. FESEM micrographs of top TCP coating (a) Low and (b) high magnification	34
Fig. 4.6. FESEM micrographs of top HAS700t2 coating (a) Low and (b) high magnification.....	35
Fig. 4.7. FESEM micrographs of top HAS800t2 coating (a) Low and (b) high magnification.....	35
Fig. 4.8. FESEM micrographs of top HAS900t2 coating (a) Low and (b) high magnification.....	35
Fig. 4.9. FESEM micrographs of top HAS1000t2 coating (a) Low and (b) high magnification	36
Fig. 4.10. FESEM micrographs of cross section TCP coating (a) Low and (b.) high magnification	37

Fig. 4.11. FESEM micrographs of cross section HAS700t2 coating (a) Low and (b) high magnification.....	37
Fig. 4.12. FESEM micrographs of cross section HAS800t2 coating (a) Low and (b) high magnification.....	37
Fig. 4.13. FESEM micrographs of cross section HAS900t2 coating (a) Low and (b) high magnification.....	38
Fig. 4.14. FESEM micrographs of cross section HAS1000t2 coating (a) Low and (b) high magnification	38
Fig. 4.15 Variation of Microhardness of TCP coating and various synthesized temperature	39
Fig. 4. 16 Variation of Scratch hardness and Fracture Toughness of TCP coating and various synthesized temperatures at load of 4N.....	40
Fig. 4. 17 (a) Variation of COF and (b) Variation of tractional force against travelling length at 4 N constant load for TCP coating.....	41
Fig. 4.18 (a) Variation of COF and (b) Variation of tractional force against travelling length at 4 N constant load for HAS700t2 coating.....	41
Fig. 4.19 (a) Variation of COF and (b) Variation of tractional force against travelling length at 4 N constant load for HAS800t2 coating.....	42
Fig. 4.20 (a) Variation of COF and (b) Variation of tractional force against travelling length at 4 N constant load for HAS900t2 coating.....	42
Fig. 4.21 (a) Variation of COF and (b) Variation of tractional force against travelling length at 4 N constant load for HAS1000t2 coating.....	43
Fig. 4.22. Variation of Specific wear rate of TCP coating and various synthesized temperature.....	44

LIST OF TABLES

Table. 1. Process parameters of plasma spray process	18
Table. 2. Chemical composition of titanium alloy.....	18
Table. 3. Sample codes of deposited coatings.....	20

ACRONYMS

APS: Atmospheric Plasma Spraying

XRD: X-Ray Diffractometer

FESEM: Field Emission Scanning Electron Microscopy

VHN: Vickers Hardness Number

HVOF: High-Velocity Oxy-Fuel

HAS: Hydroxyapatite synthesized

Chapter 1:

Introduction

1.1 Research Background:

Emerging technologies now comprise some of the most significant ongoing efforts targeted at improving surface quality through the use of various technologies. As a result, components degrade more quickly as the parts fail to withstand the demands of harsh working circumstances, and the industry's economy has suffered as a result. Material damage has been linked to faster deterioration and eventual failure of parts in a wide range of situations, including those induced by hostile environments, high relative motion between mating surfaces, corrosive fluids, and extreme temperatures.

As a result, it became important to conduct research into novel fabrication materials. It is also concerned with extending product life and improving product quality, as well as failure analysis and damage prevention of new coating materials and components. The development of a suitable high-performance coating with sufficient greater mechanical strength on a metal/alloy component offers a viable means of addressing both the bulk and surface characteristics requirements of nearly all envisioned applications.

1.2 Surface Coating:

Surface coating is the process of modifying the surface of the material to enhance its properties. It enables strong bonding at the substrate–coating interface and can offer enhanced performance and long-term stability to a substrate. Surface coating is a material addition process used for manufacturing machine tools and machine components, enhancing the desired properties such as corrosion resistance, wear resistance, good adhesion, hardness, toughness etc. This is the treatment of the surface of the material for the requirement of the properties to perform the desired function. When a single material does not possess all the desirable qualities needed to perform the function, a surface coating is required to get the desired result.

The desired properties or characteristics required of surface coatings include:

- 1) Improved corrosion resistance
- 2) Improved oxidation resistance
- 3) Improved wear resistance
- 4) Reduced frictional energy losses
- 5) Improved mechanical properties, i.e., improved toughness and hardness
- 6) To improve the fatigue properties
- 7) To improve Stiffness

By fulfilling all the criteria, surface coatings techniques are used in various industries like aerospace, biomedical, chemical, petrochemical, machine tools, constructions etc. The main advantage of the surface coatings techniques is almost all types of materials, including metals, ceramics, polymers, and composites can be coated on similar or dissimilar materials

1.3 Thermal Spraying:

Thermal spraying techniques are surface modification processes in which melted (or heated) materials are sprayed onto a substrate surface. The feedstock (coating precursor) is heated by electrical (plasma or arc) or chemical means (combustion flame). The plasma spraying process is a thermal spraying technique, which is a relatively specialized high-temperature industrial process that utilizes electrically generated plasma to heat and melt the feedstock material. The process is capital intensive and requires significant electrical power. It offers a method of depositing a feedstock material over an underlying target material as a solid coating layer. Deposition thickness gives a wide range from a few micrometers (μm) up to several millimeters by use of a variety of feedstock materials, including metals and ceramics. The feedstock material is normally presented to the plasma torch, typically in the form of a powder or wire. This feedstock melts rapidly within the plasma gun, where the typical operating temperature is $10,000\text{ }^{\circ}\text{C}$. Powered materials are injected within the plasma (RF discharges) or the plasma jet (dc arcs), where particles are accelerated and melted, or partially melted, before they flatten and solidify onto the substrate (forming lamellae or splats), the coating being built by the layering of splats. This technique is mostly used to produce coatings on different structural materials and provides protection against corrosion, erosion, and wear at high temperatures, to change the appearance and also improve the electrical properties of the surface. Plasma spraying is extensively used in a wide range of industries like aerospace, nuclear energy, as

well as conventional industries like chemicals, textiles, plastics, and paper to develop a suitable surface coating to improve the component life span in the operating environment, mainly wear-resistant coatings in crucial components.

1.3.1 Powder Flame spray:

Powder Flame spraying is the oldest of the thermal spraying processes, a wide variety of materials can be deposited as coatings using this process, and the vast majority of components are sprayed manually. The flame spray uses the heat from the combustion of fuel gas (usually acetylene or propane) to melt the coating material, which can be in the form of powder. In the flame spray process, the fuel/oxygen ratio and total gas flow rates are adjusted to produce the desired thermal output. Jet speeds typically are below 100 m/s, generating particle speeds up to 80 m/s before impact. Externally combusted or open flame, jet temperatures are generally above 2600 °C [1].

The flame spray process typically yields 85% to 98% coating densities, depending upon coating material and technique. Fig. 1.1 shows a low-velocity powder spray process. The powder is fed into the gun either by gravity flow or by pressurized feed and carried to the gun nozzle, where it is melted and projected by the gas stream onto a prepared surface. Particle speed is relatively low (<100m/s), and bond strength of deposits is generally lower than high-velocity processes. Spray rates are usually in the 0.5 to 9 kg/h range except for lower melting materials, which have higher spray rates. Oxy-fuel powder guns are the lowest cost thermal spray equipment and are easy to set up.

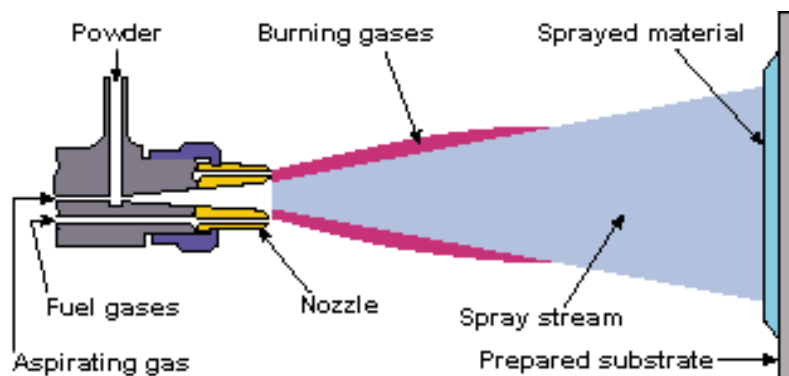


Fig. 1.1 Schematic diagram of Powder Flame Spray Process

1.3.2 Plasma spray:

Plasma spraying is a multipurpose thermal coating process. In this process, plasma is produced and controlled by a specifically designed torch by excitation of an inert gas passing through an electric arc, generating a very hot ionized gas. A unique opportunity to mix and blend materials that are otherwise incompatible is provided by the plasma spraying process. Complex alloys, elemental materials, composites, and ceramics can often be produced with this technique for use in target material fabrication. The material in the form of powder is injected into a very high temperature plasma flame, where it becomes molten and accelerated onto the substrate to provide coating [2]. Here, layer by layer, a buildup through intra-particle bonding and sintering reaction takes place. Fig 1.2 shows a Plasma spray gun that consists of an anode and cathode made of copper and tungsten, respectively, both of which are water-cooled. Plasma gas flows around the cathode and through the anode which is shaped as a constricting [3]. A high voltage discharge initiates plasma to cause localized ionization; this also generates a conductive path between cathode and anode to form a DC arc. The gas reaches extreme temperatures due to the resistance heating from the arc resulting in dissociation and ionization to form the plasma [3]. The plasma exits the anode nozzle as a free or neutral plasma flame. After the plasma is stabilized, the electric arc extends down the nozzle without shorting out to the nearest edge of the anode nozzle. The plasma arc is constricted by the cold gas around the anode nozzle resulting in higher temperature and velocity. An external powder port (near the anode nozzle) is used to feed the powder into the plasma flame.

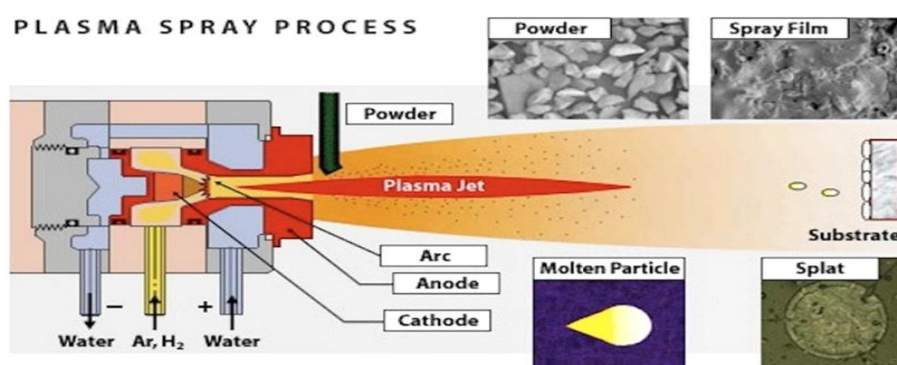


Fig. 1.2 Schematic diagram of Plasma Spray Process

1.3.3 High-velocity oxygen fuel (HVOF) spray:

HVOF spraying differs from conventional flame spraying in that the combustion process is internal, and the gas flow rates and delivery pressures are much higher than those in the flame spraying processes. In principle, high-volume combustible gases are fed into a combustion chamber, fed into a long confining nozzle, and sprayed onto the substrate with high velocities, as shown in Fig. 1.3. The volume of gas flow along with the high temperature of combustion creates gas velocities in the range of 1525 m/s to 1825 m/s. HVOF uses hydrogen, propylene, propane, acetylene, and kerosene as fuel gases.

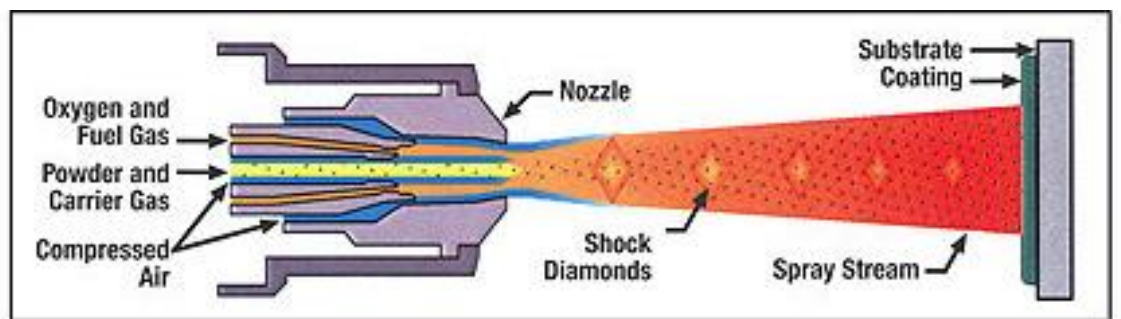


Fig. 1.3. Schematic diagram of high-velocity oxy-fuel (HVOF) spray process

Lower average particle temperature, compared to plasma spray; reduce the degree of particle melting and oxidation. Despite the lower average particle temperatures, high coating densities are still achieved through high particle impact velocities. HVOF sprayed coating density, adhesion, and oxide contents are comparable to high-energy, plasma-sprayed coatings [4].

1.3.4 Electric arc spray:

The electric arc spraying is used to spray metals in wire form; this spraying process, along with the wire flame spray, is also referred to as the metalizing process. Electric arc spraying differs from other thermal spraying processes in that there is no external heat source, such as a gas flame or electricity induced in plasma [5]. In an electric arc, heating occurs when two oppositely charged wires of sprayed material are fed together such that a controlled arc occurs between them at the intersection. Fig. 1.4 shows an electric arc spray process. The thermal efficiency of an electric arc is considerably higher than that of any other thermal spray process

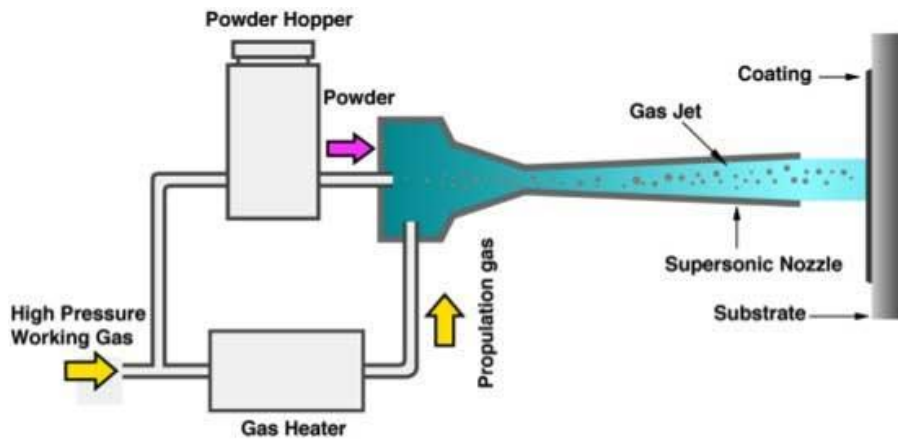


Fig. 1.5. Schematic diagram of cold spray process

1.3.6 Detonation Gun (D-Gun):

In this process, the consumable powder is pushed into the gun under small gas pressure. Valves are opened to allow oxygen and acetylene to enter the combustion chamber of the gun. The gas mixture is then detonated by igniting a spark using a spark plug, and an explosion occurs instantly. On detonation, the hot molten particles with a very high-velocity rush towards the substrate kept in front of it. The design of conventional flame spray processes limits their ability to produce dense (less than 2% porosity), well-bonded coatings. Detonation guns, however, produce higher thermal and kinetic energy jets by confining the combustion within a tube or barrel into which powders are introduced. This design produces greater heat and momentum transfer to the powder particles. Detonation spray is illustrated schematically in Fig. 1.6. In detonation spraying, an explosive mixture of fuel, oxygen, and powder is introduced into a long tube/barrel and ignited by a spark plug. The resulting detonation-pressure wave heats and accelerates the entrained powder particles, which travel down the water-cooled barrel toward the substrate. Nitrogen is used to purge the barrel between detonations. The cycle of purging, injection and detonation is repeated at a frequency of 3 to 6 Hz. Detonation spray processes are hotter and yield longer particle dwell times than conventional flame spray. High particle velocities greater than 800 m/s are generated. These high particle velocities have been shown to improve particle deformation and increase particle/coating bonding, eliminating much of the porosity typically found in conventional flame sprayed coatings.

In this process, the consumable powder is pushed into the gun under small gas pressure. Valves are opened to allow oxygen and acetylene to enter the combustion chamber of the gun. The high velocity of the particle leads to the form of a well-bonded, dense coating. As this process produces a loud noise and therefore it is recommended to perform spraying inside a soundproof

room. Apart from the gun, a detonation gun system requires arrangement for fuel and purge gas control, powder feeding, gun cooling, and spark plug operation.

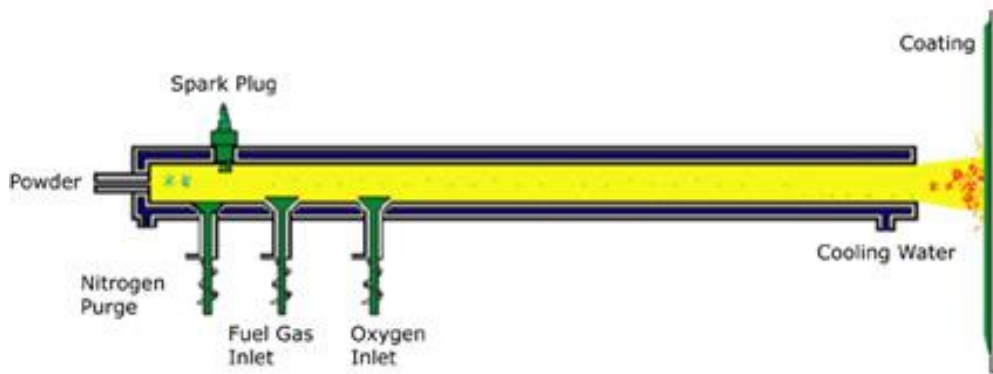


Fig. 1.6. Schematic diagram of detonation gun process

1.4 Plasma Spraying:

Atmospheric plasma spray is probably the most versatile of all thermal spraying processes because there are few limitations either on the materials that can be sprayed or the substrate in relation to its material, size, and shape [6]. The material precursor of the coating could be in the form of powders, wires, melted materials, solutions, or suspensions. What distinguishes the plasma spray process from other technologies is its applicability and capacity to process a wide variety of materials, including metallic and refractory materials at atmospheric pressure [6]. The coatings properties are improved by deposition of coatings with finer microstructure, which is more suitable for mechanical and thermal stresses than the lamellar microstructure of conventional plasma-sprayed coatings [4]. The setup of the plasma spray coating process [25] is depicted in Fig. 1.7.

The synthesis of coatings by the APS technique occurs by stacking the lamellae resulting from the impact, flattening, and solidification by the colliding molten particles [4]. The material precursor of the coating may be in the form of powders, wires, melt materials, solutions, or suspensions. APS can be applied to a wide variety of materials, including metallic and refractory materials. In this technique, a carrier gas conducts the material particles by injecting them at high velocity through the plasma, where they are molten or partially molten, taking the form of droplets that settle and solidify on the surface being coated. The material to be deposited is carried in the form of a solution or powder to a torch with sufficient enthalpy to generate a plasma jet to melt the particles [6]. The parameters of the plasma spraying process,

as well as the characteristics of the precursor (solids or liquids) used for coating, influence the properties of the deposited materials [6]. Characteristics of the coatings such as porosity, atomic structure, roughness, cohesion, and adhesion are fundamentally related to the interaction of the precursor with the plasma jet [6].

In the deposition process of plasma spray, the substrate is usually prepared to receive the coating by performing cleaning procedures (removing oils and greases), inducing surface roughness, pre-heating, and controlling movement. The adhesion of the particles to the substrate and between the lamellae strongly depends on the preparation of the substrate, pre-heating temperature, and morphology and composition of the material. Pre-heating, generally performed with the plasma jet itself, must be controlled according to the size and thickness of the part to be coated. Substrate and coating temperatures, either for pre-heating or during deposition, are linked to the residual voltage distribution, which is a controlled parameter [4].

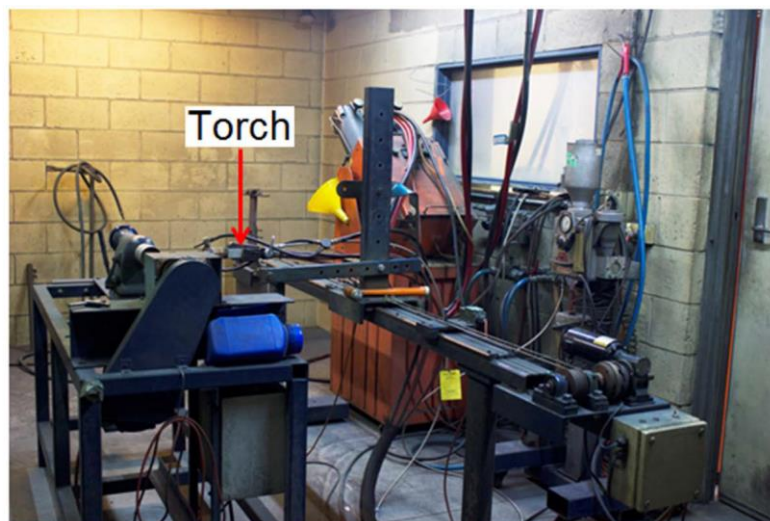


Fig. 1.7. Setup of plasma spray process [25]

1.4.1 Components of plasma spray:

1.4.1.1 Plasmatron:

It is the device that holds the electrodes and controls the plasma response. It is coupled to the water-cooled power supply cables, powder supply hose, and gas supply hose in the shape of a pistol.

1.4.1.2 The power supply unit:

Plasma arcs often operate in a DC environment with low voltage (30-60 V) and high current (300-700 Amps). The available three-phase 440V to fit the reactor. AC electricity must be changed and rectified. The power is responsible for this.

1.4.1.3 The powder feeder:

Inside a hopper, the powder is maintained. The powder is fluidized and transported to the plasma arc via a separate gas line. It is possible to adjust the powder flow rate carefully.

1.4.1.4 The coolant and water supply unit:

Water is pumped into the plasmatron, which generates electricity, power wires, and the supply unit. Refrigerated water can also be supplied by some of the units.

1.4.1.5 Control unit:

The main functionalities (current control, gas flow rate control, and so on) are all present. The control unit contains relays, solenoid valves, and other components that make up the rest of the system. For the equipment to run safely, interlocking arrangements are necessary. An arc, for example, starts if the coolant supply is turned on and the water pressure and flow rate are sufficient. The primary plasma gas is argon, whereas the secondary gas is nitrogen. The powder combination is sprayed at a 90° angle. The spray process parameters influence the qualities of the coated products. Table 1 shows the operational parameters used during coating deposition.

1.4.2 Process parameters in plasma spraying:

1.4.2.1 Arc power:

The water concentration of hydroxyapatite after manufacturing makes it unsuitable for plasma spray coating. We use a procedure known as Spray Drying to make it sprayable. The hydroxyapatite has become sprayable after spray drying.

1.4.2.2 Plasma gas:

The plasma-generating gas used has such an impact on the parameters of a plasma flame. The four most common gases are argon, helium, hydrogen, and nitrogen. Argon has numerous benefits as plasma gas. It is low-cost, easily ionized, and inert, shielding the plasma gun's powder particles as electrodes from the elements.

The main gas plays the most critical role in the gas mixture, whereas the supplementary gas plays the least important role. The molecules are attacked by electrons, which causes them to become ionized. The temperature and enthalpy of the gases rise as it absorbs a photon. Because nitrogen and hydrogen are diatomic gases, they must be separated before they can be ionized. They require higher energy input to enter the plasma state. The heat transmission rate from the plasma toward the powder particles is increased, which encourages the melting of the powder particles [7].

1.4.2.3 Mass flow rate of powder:

Mass flow rate refers to the rate during which powder is injected into the plasma flame. Mass flow rate has a direct relationship with coating thickness. Hence the higher the mass flow rate, the thicker the coating. The mass flow rate of the powder is not too high or low. Incomplete melting happens when the mass flow rates are so high, resulting in large porosity and layer thickness, which takes a very long time to solidify and includes residual stress, resulting in coating breaking. Coating formation thickness is too thin if the mass transfer rate is too low [8].

1.4.2.4 Powder related variables:

The size of the metal powder affects the plasma flame's melting capabilities. Large particles in the atmospheric plasma flame are predicted to melt more slowly than small particles. Particles with a diameter greater than 55 μm were crystal and melted very little when plasma was sprayed. The sizes of a partially melted particle with amorphous and crystalline phases range from 55 to 30 μm . Particles with a diameter of less than 30 μm were entirely melted and exhibited a variety of amorphous phases [10].

The size of particles has an impact on their velocity as they pass through the plasma flame. The maximum velocity of larger particles takes longer to reach than that of smaller ones. As they collide with the substrates, smaller particles solidify faster than bigger ones. Particle size is restricted due to the speed that particles should have in order to penetrate the plasma jet. [10].

In the process of coating creation, the particle size of the powder is critical. It will vaporize if the particle size is minimal. A massive particle, on the other hand, would be unable to melt much and so deposit. As a consequence, the powders will be a perfect size, neither too little nor too large. Powder with a particle size of 15-30 μm is ideal for coating production.

1.4.2.5 Spraying angle:

One of the most critical factors to consider while spraying is the angle. It is in charge of splat formation. Different angles were chosen based on the material (ductile and brittle material of substrate).

1.4.2.6 Substrate cooling:

The substrate may become heated during continuous spraying, causing Coating peel-off and thermal stresses. This is particularly true when applying thick deposits. A backup air supply system ensures that you do not run out of air and that the substrate cools to keep it from overheating. The cooling air jet also helps to minimize porosity by eliminating unmelted material from the surface of the coating [11].

If the substrate is not properly cooled, residual tensions in the coating will develop. Residual strains in any coating applied by thermal spray techniques are invariably formed due to differences in thermal properties between the coat and the substrate material. Variable temperature ranges faced by different areas of the component at different times throughout the process, as well as variations in the coefficients of thermal expansion of the various stages within the coating material, further complicate the method. Coating cracks arise when residual tensions are present [11]. The temperature of the plasma flame, the properties of the sprayed particles, the temperature of the substrate, and the cooling effects are all elements that impact the formation of residual stress. The coating thickness has an impact on residual stress. As the number of levels grows, residual stresses increase. The chosen pre-heat temperatures must be low enough to prevent the substrate from being damaged [11].

1.4.2.7 Angle of power injection:

Coating Powders could be injected into the plasma jet perpendicularly, coaxially, or obliquely. For a given carrier gas flow rate, the powdered material residence time varies with injection angle. The degree of melting of a particular powder will be influenced by the residence time. To melt higher melting materials, for example, a longer residence time is required; hence oblique injection may be preferable.

1.4.3 Requirements for Plasma Spraying:

For coating the material, we can also use different types of thermal spray processes depending upon the type of application. The plasma spray process is the only unique process used in orthopedic applications, approved by the World Health Organization. The plasma spray process has various advantages rather than another thermal processes.

Chapter 2

Literature Review

This chapter presents the review of the past work on thermal spray-based coatings, the identified research gaps, the research objective to bridge fill in the gaps in the study, and the research technique that has been discovered and used in the present work.

2.1 Plasma spray processes for different coating materials:

1. **Kazi Sabiruddin** and **Shahid Hussain** have prepared the synthesized hydroxyapatite powder from the Indian clam seashell. By taking the seashell and the ball milling process is used for crushing the seashell and then heat-treated at several temperatures 700, 800, 900, 1000°C for the different time periods 1, 2, and 3 h. And then, they concluded that the maximum amount of crystalline HA could be obtained by applying a heating temperature of 900 °C for 2 hours.

2. **Jarnail Singh** et al. analyzed the characterization of plasma-sprayed calcium silicate coating. They concluded the addition of calcium silicate in hydroxyapatite in the coating (HA-CS coating) has a stronger microhardness than the others and exhibits significantly higher microhardness than pure hydroxyapatite coating. The surface roughness and porosity of HA-CS coating are higher than the pure HA coating. The surface of the HA-CS coatings demonstrated crack-free surface morphology, where microcracks are observed over the surface of pure HA coatings.

3. **Gurpreet Singh** et al. analyzed the Improvement of surface properties and corrosion resistance of titanium alloy by plasma-sprayed HA and ZnO coating and concluded that a progressive increase in microhardness occurs with the rise of ZnO reinforcement in HA and ZnO coated samples and delivers the maximum hardness, while pure HA-coated sample yields the lowest hardness.

4. Renu Kumari et al. analyzed the Microstructure and surface mechanical properties of plasma spray deposited and post spray heat-treated hydroxyapatite (HA) based composite coating on titanium alloy and concluded that Post spray heat treatment reduces the area fraction of porosity and Improved hardness after post heat treatment as compared to as-sprayed coating.

5. Y.C. Yang et al. analyzed the Bonding strength investigation of plasma-sprayed HA coatings and concluded that the bonding strength of the post-heat-treated coating was found to increase as compared to that of pure HA coatings and the bond strength of the coating increased with the heat-treatment temperature mainly contributed by the sintering occurred in HA coating.

6. Guohomng Wang et al. analyzed the microstructure of micro-plasma sprayed hydroxyapatite coatings after post-heat treatment and analyzed the impact of heat treatment on crystallinity, microstructure, and surface morphology of HA coating. The experiment shows that the heat treatment led to the formation of grains on the coating surface. With the increase of the holding time, the particles become coarse so that it affects hardness and strength, i.e., the hardness and strength of the coating are increased, and the material tends to become brittle.

7. Manoj Mittal et al. analyzed the effects of post-heat treatment on surface roughness, residual stresses, and micromorphology properties of plasma-sprayed pure hydroxyapatite and Aloxite reinforced hydroxyapatite coatings were examined and placed on titanium alloy. It was discovered that HA coating contains some unmelted, partially melted, and entirely melted HA particles, as well as tiny surface fissures. Minor cracks form as the HA coatings cool and solidify, causing localized stresses. The microstructure of the heat-treated HA coating was similar to that of the as-sprayed coatings, with the exception that the fissures on the coating surface enlarged following the heat treatment.

2.2 Objectives:

The following are objectives formulated based on literature review observation:

1. To deposit the various spray-dried synthesized HA powders on titanium alloy substrate by using the atmospheric plasma spray coating technique.
2. Physical, mechanical, and tribological tests are performed to characterize the coated samples.
3. The crystalline phase, microstructure, roughness, and hardness of coated samples are analyzed through XRD, FESEM, stylus profilometer, and Vickers microhardness tester, respectively.
4. The coated samples are also characterized in terms of wear loss, porosity, and adhesion by using a ball-on disc tribometer, Image J software, and scratch test, respectively.

Chapter 3

Materials and Methods

This section discusses the techniques and procedures used in this study. The plasma spray system is discussed first, with every component thoroughly categorized. Following this, details of coating and materials of a substrate for using this research work are provided. This section discusses the processes used to characterize the substrate material and the analysis of the HA coatings created in this study.

3.1 Plasma Spraying:

The atmospheric plasma spray deposition is done at the Indian Institute of Technology, Patna. A standard atmospheric plasma spraying setup is employed. By regulating the gas flow rate, voltage, and arc current, the input power level of the plasma torch is 35 kW. The powder is injected outside of the nozzle and into the plasma. As a carrier gas, a combination of argon and hydrogen plasma is employed. A consistent powder feeding rate of 10 g/min was maintained using a turntable style volumetric powder feeder. A four-stage centrifugal pump with a closed-loop is utilized to cool the system with a 10kg/cm² supply pressure. Fig.1.2 and 1.7 depicts a schematic diagram depiction as well as a typical layout of equipment for the atmospheric plasma spraying process.

3.2 The Plasma Spraying System:

Major components of the plasma spray system are the plasma cannon, powder feeder, and control unit. Sulzer Dual Plasma Spray Gun was used to create the plasma. Plasma guns are typically simple in design, consisting of a chamber and a front nozzle aperture (anode). Both the nozzle and the chamber are cooled by water. At the back of the chamber is another water-cooled electrode. This non-consumable back electrode is composed of throated tungsten. The high-pressure plasma-producing gas (or gases) enters the chamber through a port. A high-frequency spark initiates the operation, which is then switched off when the ignition is turned on.

The high-pressure gas cools the outer layer of the plasma arc, preventing severe heat from reaching the nozzle bore. Plasma-forming gases include argon, nitrogen, hydrogen, and helium. They can be used individually or in combination, for example, argon-hydrogen, argon-helium, nitrogen-hydrogen, and so

on: argon-hydrogen, argon-helium, nitrogen-hydrogen, and so on. As primary and secondary plasma gases, argon and helium are often utilized. These are some parameters used for the Plasma Spray process shown in Table 1.

Table. 1. Process parameters of plasma spray technique

Parameters	Values
Plasma Power (kW)	35
Stand Off Distance (mm)	100
Powder feed rate (g/min)	10
Primary gas flow rate, Argon (SCFH)	65
Secondary gas flow rate, Hydrogen (SCFH)	6

3.3 Materials:

3.3.1 Substrate:

Titanium alloy was employed as a substrate for HA plasma spraying. The biocompatible titanium alloy Ti6Al4V is the commonly utilized material for HA coating for bone replacements. The substrate materials were obtained in the shape of a rectangular size (25×25×5 mm³). The chemical composition of titanium alloy is shown in Table 2.

Table. 2. Chemical composition of titanium alloy

Element	Ti	Al	V	Fe
Composition (wt %)	89.5	6.4	3.89	0.16

Titanium alloy implants would provide strong bone-implant attachment under human physiological stress conditions, allowing for a high rate of fracture [17]. Titanium alloys offer desirable qualities such as high strength, outstanding high-temperature mechanical capabilities,

and superior corrosion resistance [16]. It has a high melting point and low coefficient of thermal expansion [16].

3.3.2 Coating material:

Plasma spray coating employs hydroxyapatite as the coating material, which is commonly used to connect bones in biomedical applications since it meets all material criteria, including acceptable specifications [18]. Phosphate has been the most prevalent naturally occurring element on the planet. It contributes significantly to the global phosphorus cycle as a source of phosphorus. It is also known as hydroxyapatite [23-24], calcium hydroxyapatite, and it is composed of the same materials as bone [19].

Commercially available hydroxyapatite is also available, but it lacks the characteristics and combination of titanium alloy that we want for biomedical applications; thus, we use synthetic hydroxyapatite. The method called hydrothermal method is used to make hydroxyapatite from Indian clam seashell [21].

3.4 Substrate Preparation:

3.4.1 Grit Blasting:

The substrate is grit blasted before atmospheric plasma spraying to make the surface rough, which effectively increases the bonding strength of coating and substrate. The titanium alloy was grit blasted with 500 μm (mesh 24) pure white alumina. It is often used in therapeutic applications due to its biocompatibility. For grit blasting, a blasting pressure of 5 kgf/cm^2 was applied. The samples were grit blasted for one minute to verify that the requisite surfaces were roughened. A 90-degree angle of incidence and a 100-mm standoff distance is employed for grit blasting.

3.4.2 Substrate Cleaning:

The substrate must be cleaned with acetone before spraying, a procedure known as ultrasonic cleaning. Ultrasonic cleaning removes all pollutants from the substrates, such as rust and

external contaminants from a surface. Isopropyl alcohol is utilized as a solvent in ultrasonic cleaning, and the substrate is kept in the container for around 5 minutes. The spray is essential after grit blasting. Otherwise, there could be oxide coatings on the surfaces, as well as dampness. The coating quality will suffer as a result, and ambient gases will be trapped in the coating. This causes porosity to occur in the coating, lowering the strength of the coating. After the plasma spray process, the following coated samples are prepared, which are shown in Table 3.

Table 3. Sample codes of various deposited coatings by plasma spray process

Sample Codes	Description
TCP	Tricalcium Phosphate Coating
700	HAS700t2 Coating
800	HAS800t2 Coating
900	HAS900t2 Coating
1000	HAS1000t2 Coating

3.5 Characterization of Coatings:

3.5.1 X-Ray diffractometer (XRD):

The distinct phases (elemental phase/intermetallic process phase/non-crystalline phase) that exist in the coating were recognized using the X-ray diffraction method. The X-ray diffractometer setup is depicted in Fig. 3.1. An XRD (Rikagu Smart Lab) was used to conduct the study. The XRD uses Ni-filtered Cu-K radiation ($\lambda = 0.15406$ nm) at 30 kV and 40 mA. The distinct X-ray peaks were determined by comparing the d-values acquired from XRD analysis to the typical d-spacing of all conceivable values from JCPDS cards.

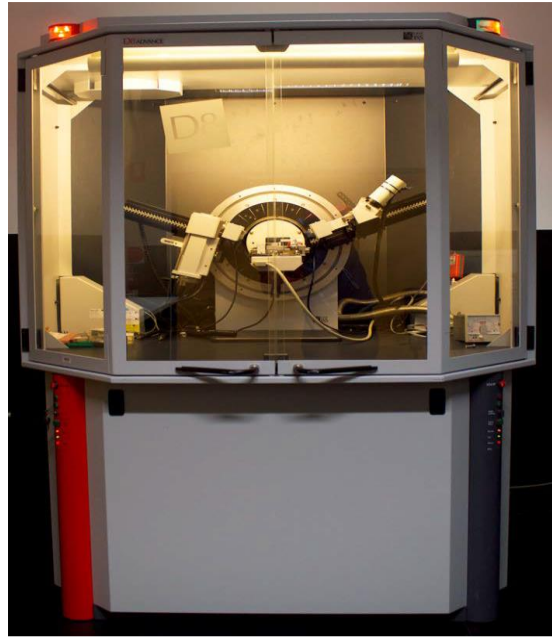


Fig. 3.1. Setup of X-ray diffractometer [25]

3.5.2 Roughness Measurement:

A profilometer allows the measurement of surface roughness. The surface roughness of the coatings was measured using the Surtroic 25 (Taylor Hobson, UK) profilometer, shown in Fig 3.2. This is a 2D profilometer that has a stylus that is run over the surface of the coating. Accuracy of the roughness tester was checked prior to the measurement with a calibration sample. The surface roughness (R_a) of the coating was determined using Taylor and Hobson contact type Stylus Profilometer. This equipment consists of a stylus that is run over the surface of the coating. The sample was held in place using tape to prevent movement during measurement that would lead to inaccuracy. Three measurements were taken for each sample, and then the average of these was determined.

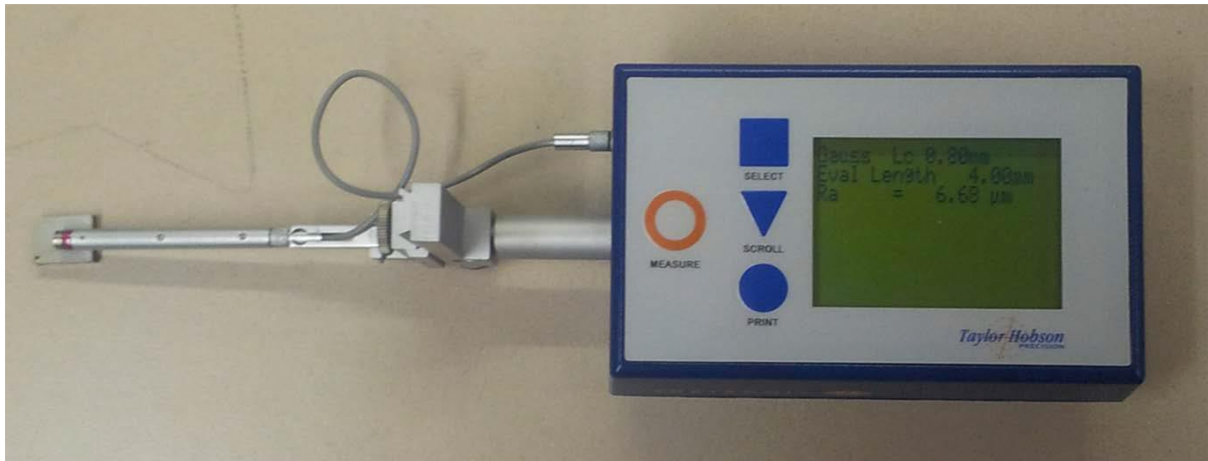


Fig. 3.2 Setup of Taylor and Hobson profilometer

3.5.3 Mounting, Grinding, and Polishing:

3.5.3.1 Specimen sectioning:

The coated samples are segmented using an automated cutter so that their cross-sections can be examined. A highly precise cutting tool (Secotom 15, Struers) was used to segment sample Fig. 3.3.



Fig. 3.3. Setup of high-speed cutter

3.5.3.2 Cleaning:

Samples are cleaned using freshwater or even other cleaning solutions to extricate the entrapped particles. After sectioning, it is vital to dry the specimen to ensure that the mount and the specimen remain untouched.

3.5.3.3 Specimen mounting:

Cleaned samples are hot mounted to hold firmly during the polishing for performing the various physical and mechanical tests. Buehler resin is employed in the hot mounting process. In a hot mounting press, the mold is filled with resin by caring for the proper sample orientation.

3.5.3.4 Grinding:

Grinding is being used to make flat mounting samples and to remove the burrs or any irregular material on the specimen.

3.5.3.5 Polishing:

The specimens were wet polished using papers of grades 220, 400, 600, 800, 1000, 1200, 1500, and 2000 after they had been ground. All samples are diamonds polished to less than 1 μm roughness after wet polishing.

3.5.4 Thickness Measurement:

A specimen cross-sectional area was polished and examined using inverted microscopy to determine the thickness of coated surface on the substrate. The thickness of coatings was measured using micrographs of polished samples. These measurements were made with the image analysis software. A measuring bar was added to the picture to determine the thickness. This measurement was performed at six sites to the length of the coating to minimize measurement error, and the average value is presented as the (mean) coating thicknesses.

3.5.5 Microstructural Study of Coating:

Plasma spray-coated specimens, polished cross-sections, and powder. A scanning electron microscope was used to examine the morphology. (FESEM or SEM, JEOL JSM 7610 Plus). The samples tested for SEM should be appropriate to fit inside the SEM specimen vacuum chamber. HA is a non-conducting material. Thus, the surface of the sample must be electrically conductive; otherwise, charging effects may arise during scanning. Thin gold coatings are widely used to make the surface conductive. All samples studied in this research were gold coated with a DYNAVAC deposition system prior to the SEM analysis.

The sample was mounted on a sample holder using a carbon tape that made a connection between the sample holder and a thin gold coating. After completion of gold sputtering, the sample was placed under the SEM observation as quickly as possible. The sample was kept in a vacuum between the gold sputtering and SEM observation. Using an X-ray diffractometer (Rigaku Smart Lab 3 kW) with CuK radiation operating current of 40 mA and accelerating voltage of 30 kV, the phases contained in seashell powder, temperature seashell, and hydrothermal reaction products are examined. For the 20–60 angle range, a scan speed of 2/min with a scale factor of 0.02 is used. The Scanning Electron Microscopy machine is shown in Fig.3.4.



Fig. 3.4. Setup of Scanning Electron Microscope [25]

3.5.6 Porosity Measurement:

The porosity of a coating is an important factor that describes the inherent characteristics of the coating. Porosity is most important for orthopedic applications. The level of porosity required depends on the application. To obtain good mechanical properties, a porosity of less than 5% is preferable. The porosity is to be evaluated from high-resolution images from a microscope of the area of the cross-section of the coating. Image processing and analysis in Java (ImageJ) software were used to calculate the porosity. The pores inside the coating may be highlighted with this program, and the software can then determine the porosity fraction of the coating. First, it is necessary to set up the scale of the image. Secondly, the threshold value needs to be adjusted so that all the pores are highlighted. The image then needs to be smoothed to resolve the pores. After that, particles are analyzed to measure the area fraction or porosity of the coatings.

3.5.7 Microhardness Measurement:

Sample preparation is important for this test to provide a small sample that can be placed into the tester. The sample tested surface needs to be smooth since the measurement system is optically based. The indentation should be large enough to maximize the measurement resolution. Error percentages decrease with an increase in indentation sizes. In this test, vertical and horizontal axes are measured after indentation. Then, this measurement is converted to a Vickers hardness number, using the following formula

$$\mathbf{VH = 1.8544 P/d^2}$$

Where d is the average of the two diagonals d_1 and d_2 in millimeters, P is the applied force in kgf, and VHN is the Vickers hardness number.

Indenting the test items with a diamond indenter in the shape of a pyramid with a square base as well as an angle of 136 degrees between opposed sides is the Vickers hardness test technique. Vickers hardness measurements were performed using a Leitz Micro hardness tester with a display and a microprocessor-based controller at a load of 50 gf for 15 seconds. After the load has been removed, the two diagonals of the depression left on the surface of material are measured, as illustrated in Fig.3.5.

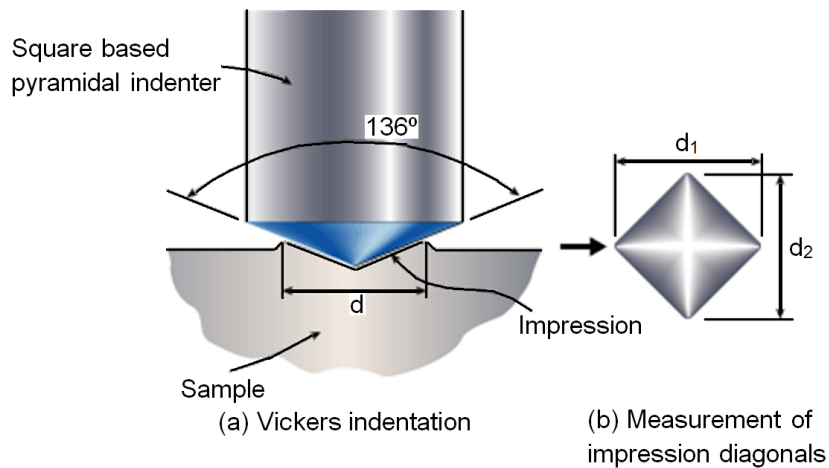


Fig. 3.5. Schematic diagram of Vickers's Hardness test

3.5.8 Scratch Analysis:

A scratch testing machine (DUCOM, TR-101) with a diamond indenter (Blue Star, apex angle: 120°, tip radius: 200 μm) would be used to evaluate the scratch hardness and fracture toughness. All scratch tester tests are performed in a temp and relative humidity environmental condition of 26°C and 54%, respectively. The morphological properties of the coatings are examined using an inverted microscope (Leica, DFC295). The Fracture toughness can be evaluated by the following equation [24].

$$\text{Fracture Toughness} = K_c = \frac{F_T}{\sqrt{(2pa)}}$$

where

$$2pa = \frac{4 \tan \phi}{\cos \phi} d^3 \qquad d = \frac{w}{2 \tan \phi}$$

F_T = Traction Force (N)

F_N = Normal Force (N)

ϕ = Half apex angle of conical indenter (degree)

d = Penetration depth (mm)

w = Scratch width (mm)

The Scratch Hardness can be evaluated by the following equation

$$\text{Scratch Hardness} = H = \frac{8F_N}{\pi w^2}$$

3.5.9 Wear Analysis:

Wear tests on the coatings were performed at atmospheric temperature with a Ball-on-disc tribometer. Sliding ball-on-disc tests were conducted on each coated disc under non-lubricated (dry) conditions. The test pair used was Co-WC balls, 6 mm in diameter as a counter body. The coated sample has dimensions (25×25×5 mm), ground to an average surface roughness of below 1 μm. The tests were conducted at a 5 mm track diameter and 100 rpm and a sliding distance of 23.47 m. A 1 kgf load was used in all tests at a time of 15 min. The frictional forces and coefficient of friction values were continuously recorded on a computer and sampled at a frequency of 1 Hz. The ball-on-disc wear test setup is shown schematically in Fig. 3.6. At the end of each test to calculating the area to compute the volume loss in order to determine the particular wear rate using the wear track from a profile trace taken by a contact type stylus profilometer (Taylor Hobson, Surtronic 25).

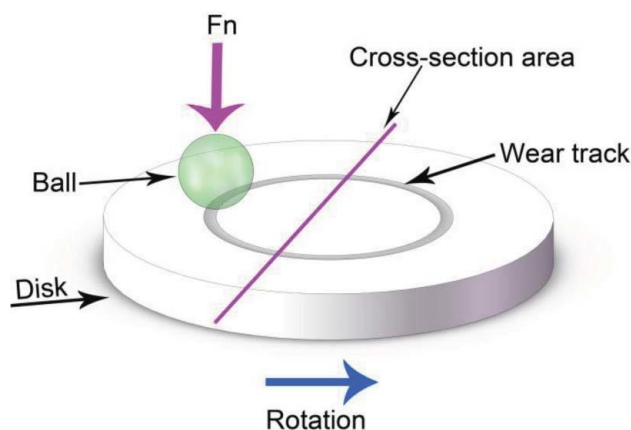


Fig. 3.6. Schematic diagram of Ball on Disc Test

Using the equation below, the wear rate is calculated.

$$SWR = (V/dL) * 10^{-9}$$

where,

SWR = Specific wear rate in m/(N·m)

d = Sliding distance unit in m.

L = Normal load in N.

V = Volume of wear track in millimeter.

Now,

$$V = \pi \cdot d_w \cdot A$$

where,

d_w = diameter of wear track in mm.

A = cross-sectional area of wear track in mm².

The wear scar just on tested sample is thought to resemble a circular section. The following equation may be used to calculate the cross-sectional area of worn track 'A'.

$$A = R^2 [\sin^{-1} (h_T/2R)^{0.5} - 0.25 \sin \{4 (\sin^{-1} (h_T/2R)^{0.5})\}]$$

where,

h = average wear depth track in mm.

R = Radius of WC ball in mm.

Chapter 4

Results And Discussion

Different synthesized HA are coated on titanium alloy substrate by using the atmospheric plasma spray method. The coatings were characterized, and the tribological properties of the coatings were studied. This chapter presents and discusses the findings of several tests.

4.1 XRD analysis:

Fig 4.1 shows the XRD results of the coating, indicating that the different phases present and primary phases are HA, calcium oxide, and tri calcium phosphate. In the graph, the major peaks of each phase are labeled. The coating contains some calcium oxide compounds, according to an XRD study. The temperature of the synthesized material is raised from 700 °C to 1000 °C, a phase transformation, implying the raw material and coating. The XRD graph shows that the formation of CaO is more in the HAS900t2 sample compared to the other coatings samples. And in the HAS900 sample, it has some phases of tricalcium phosphate and calcium oxide along with the hydroxyapatite, which makes the material tends brittle.

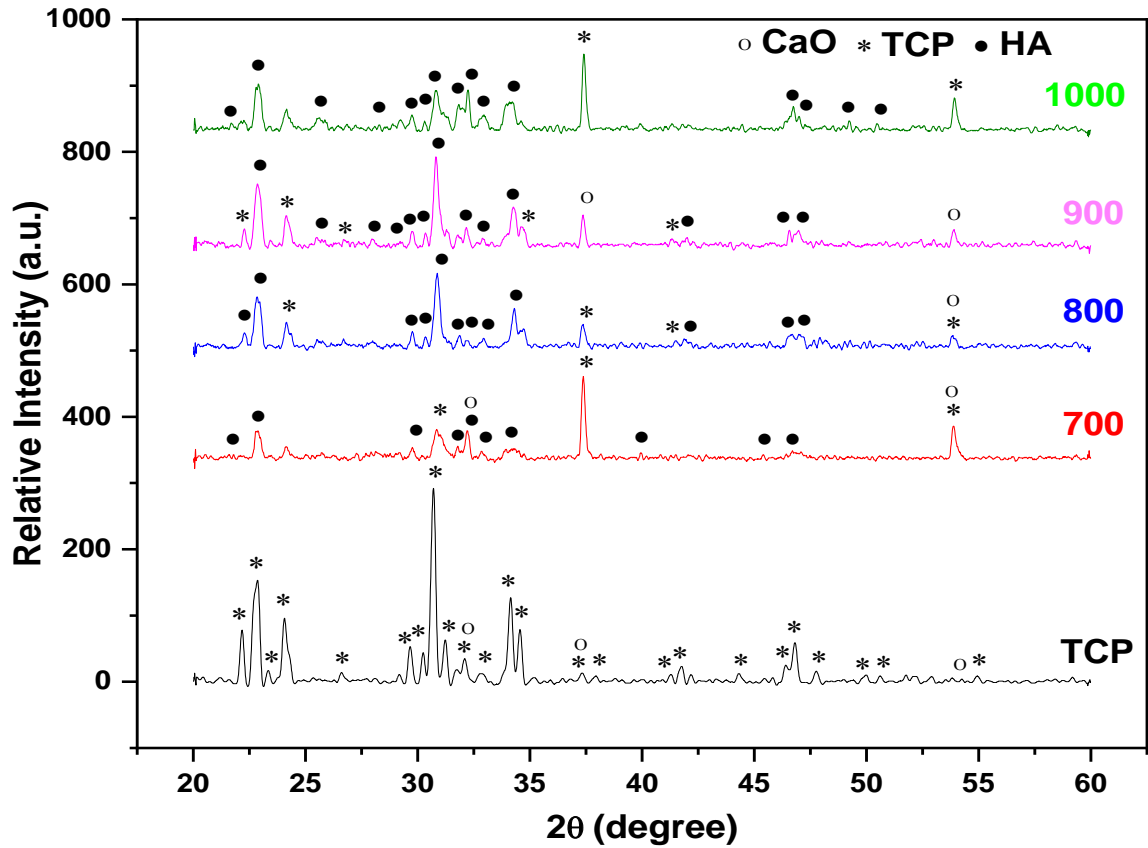


Fig. 4.1. XRD patterns of TCP coating and synthesized at various temperatures HA coating

4.2 Thickness Measurement:

The thickness of hydroxyapatite coatings is analyzed with the help of an inverted microscope to quantify the polished cross-sections of the samples. The data point for each curve is the mean of five trials. For the HAS700t2 sample, the maximum thickness of the coated sample is 496 μm . The range of thickness values for coating samples is shown in the Fig. 4.2. The deposition of particles in the thermal spray of coatings created using the APS process is influenced by the synthesis temperature of hydroxyapatite powder. As the temperature rises, a greater number of particles melt, and it is limited to a certain range of temperatures. When these molten species come into contact with the substrate, they flatten out and cling to the surface, forming enormous splats. Thickness is reduced when the bonding among these splats is strong, and the area of

contact between the droplets and the substrate is greater. As a result, even though the thickness is reduced, a dense coating is generated.

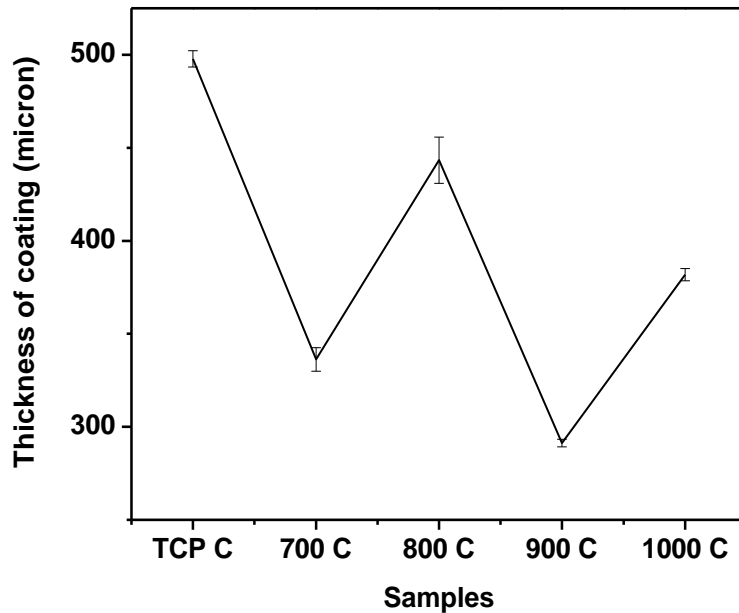


Fig. 4.2. Thickness value of TCP coating and at various temperatures synthesized HA coatings

4.3 Roughness Measurement:

The results, as shown in Fig. 4.3, show that raising the heat treatment temperature reduced the surface roughness of coating from HAS700t2 sample. This is occurring due to the proper timing of melted droplets hitting the substrate and splats ideally with respect to the other upcoming droplets. The following tendencies are found by raising the synthesized temperature. Due to the change in cooling rate, proper splat formation takes place. As a result, roughness decrease. This behavior is most likely owing to the impacting droplet's increased wettability of its flattening on the substrate. For increasing synthesis temperature, proper melting behavior is also obtained. For increasing synthesis temperature, a less number of unmolten particles and semi-molten particles are observed, which gives proper melting of the particles, then reduces the surface roughness of the coating. The very low value of surface roughness is obtained in the case of 1000 samples, around 6.432 μm , as compared to all other samples.

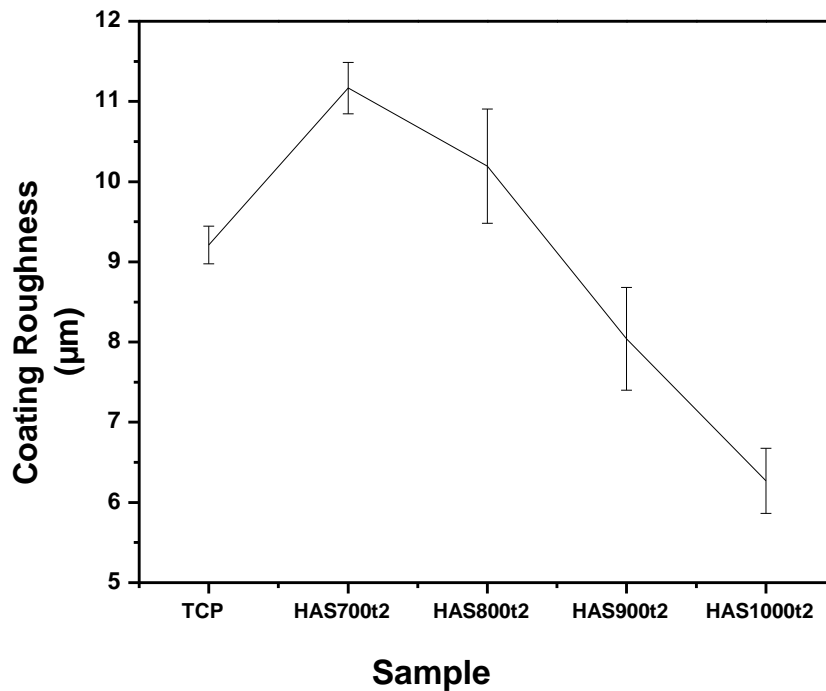


Fig. 4.3. Roughness value of TCP coating and at various temperatures synthesized HA coatings

4.4 Porosity Measurement:

The porosity was examined and used the image J software evaluation technique. FESEM images of various coated samples are considered for porosity measurement in terms of area percentage. The amount of entrapped gas in the pores/inter-splat area has a major impact on the porosity of the coating. As the coating thickness increases, the porosity changes. This is due to the thermal treatment effect, which is most noticeable at the top layer of the protective layer as a result of the high-temperature exposure. The top layer exhibits the biggest transition from metastable to stable phases, as well as the most pore suppression. As a result, the coated samples have the highest porosity in the deep areas and the lowest porosity at the top.

Fig. 4.4 demonstrates the variation in hydroxyapatite coating porosity with respect to various obtained coated samples. Surface porosity is higher in coatings obtained at 800 °C synthesized powder sample and gradually reduces as the temperature rises from 800 to 1000 °C. The low bonding strength of the coatings results in increased porosity. For all samples, variation in the

coating porosity is observed. This is due to morphological and spatial differences in splats, which range from entirely flat and well adherent to coarse and poorly adhered. Furthermore, the amount of hardened particles increases, promoting the formation of gaps surrounding them because these particles remain practically spherical in shape and are unable to flatten to fill the valleys. Other approaching droplets will have a hard time filling up around these particles without creating voids [22].

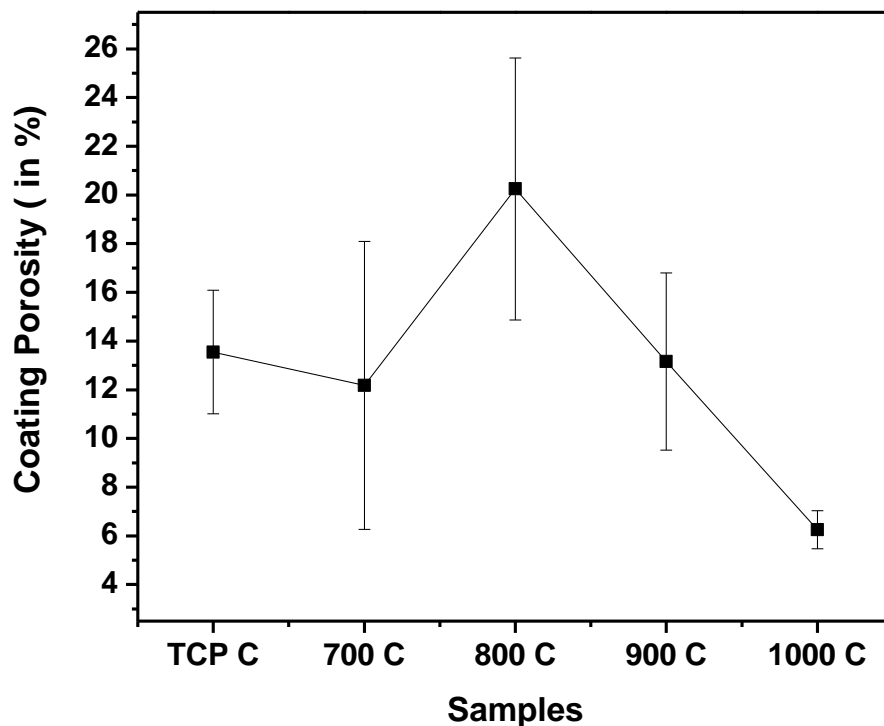


Fig 4.4 Variation of Porosity of TCP Coating and at various synthesized temperature HA coatings

4.5 Microstructural Study of the Coatings:

4.5.1 Top Surface Morphology:

The microstructural property of coating depends on the morphology and bonding between particles of the sprayed powders. FESEM micrographs of HA coating surfaces are shown in Fig. 4.5-4.9. More cavitation is noticed in the tri calcium phosphate (TCP) coating. As it is clear from FESEM image, as shown in Fig 4.5, TCP coating shows that there is a large number

of droplets agglomerating and causing to increase in surface roughness and porosity and tending to decrease the hardness. On the inter-particle borders and at grain intersections, certain open pores can be observed. These might have resulted from insufficient molten particle flow during solidification, as seen in Fig 4.7- 4.9. The coating formed at 700 °C and 800 °C temperatures, as shown in Fig. 4.8-4.9 has a distinct shape, with some spheroidal splats indicating full melting of particles during plasma jet transit. Inter-granular borders have less cavitation than granular boundaries. The coating obtained at 1000 °C synthesized temperature, as shown in Fig 4.9, displays a homogeneous dispersion of molten/semi-molten particles that have agglomerated. In the case of the coating obtained at 900 °C and 1000 °C synthesized temperatures, as shown in Fig 4.8-4.9, the particles get more thermal energy, so during solidification from the molten state, they agglomerate to form splats, i.e., flattened region. Here very less amount of cavitation is observed. This may be the reason for better interface adhesion of the coating onto the substrate, leading to increased adhesion strength. Morphology of these samples also shows a uniform distribution of molten/semi-molten particles, hence an increment in adhesion strength [23]. The uniform distribution of the droplets shown in Fig. 4.9 shows that the tendency of agglomeration is very less as compared to the other samples. The higher synthesizing temperature is responsible for a greater number of droplets melting, and these droplets come in contact with the substrate. They flatten out and cling to the surface. Fig 4.8-4.9 show that the tendency of agglomeration is decreased with respect to increasing the synthesizing temperature, and better splats formation takes place.

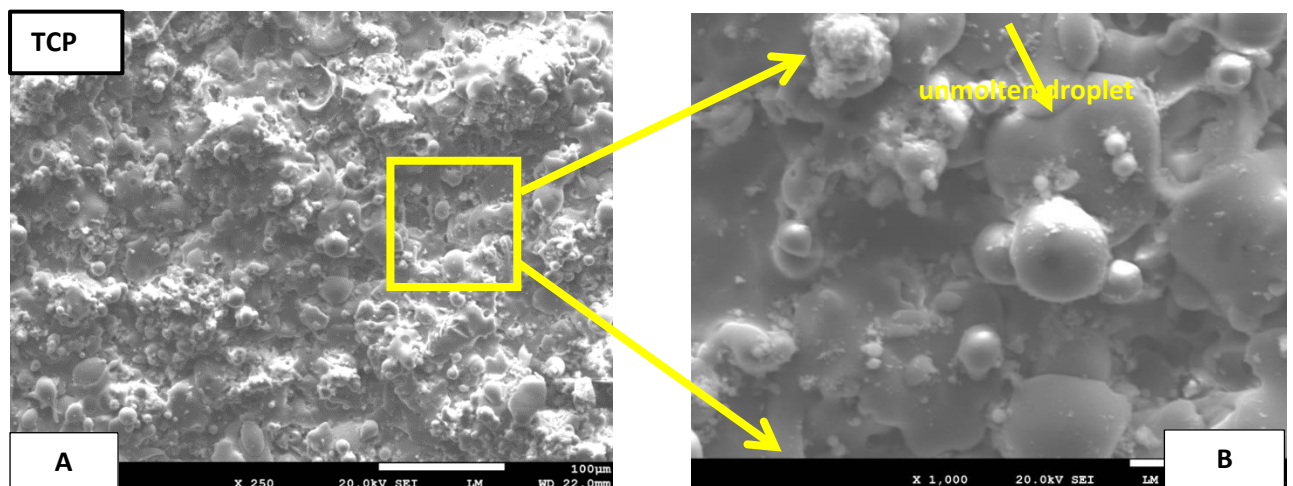


Fig. 4.5. FESEM micrographs of top TCP coating (a) Low and (b) high magnification

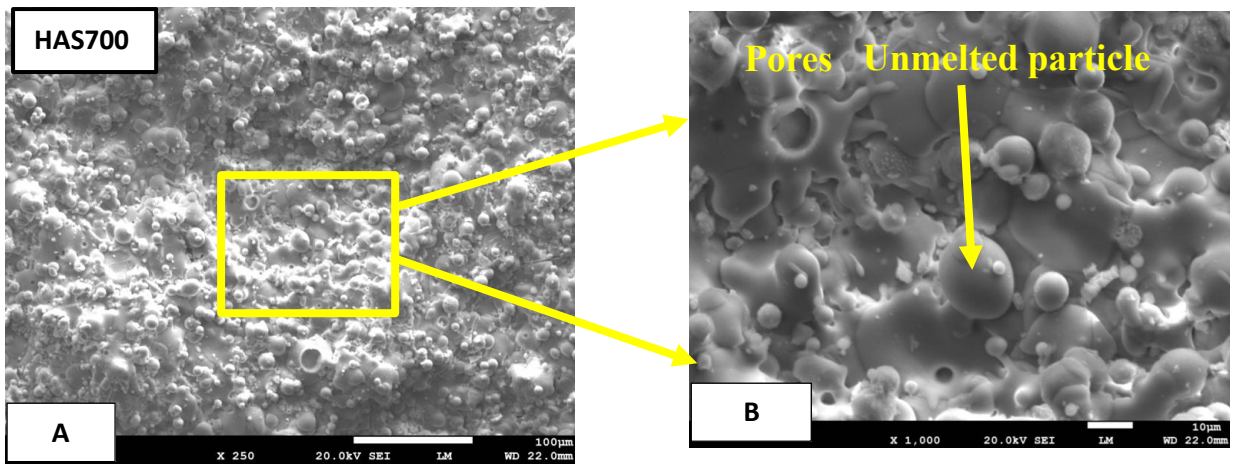


Fig. 4.6. FESEM micrographs of top HAS700t2 coating (a) Low and (b) high magnification

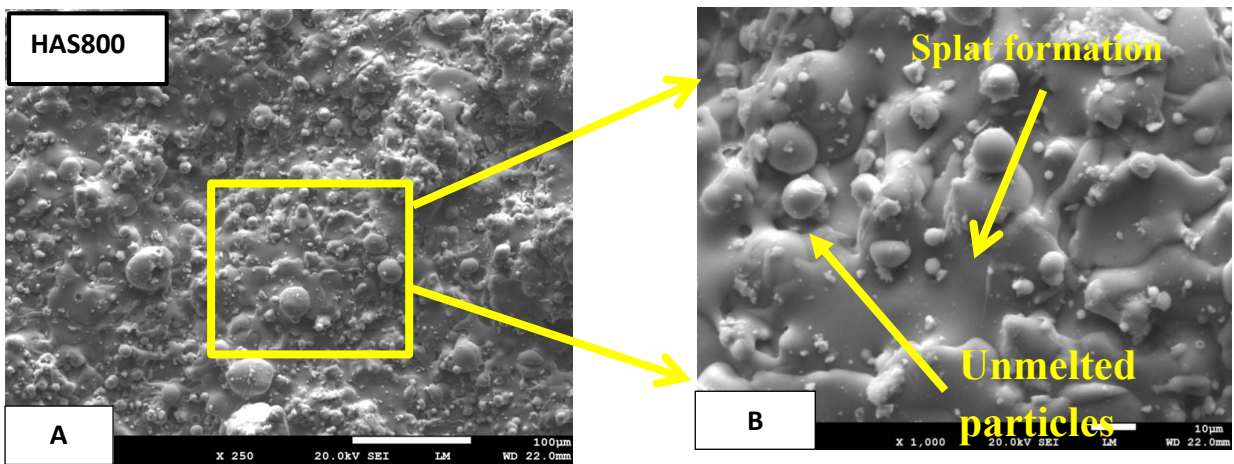


Fig. 4.7. FESEM micrographs of top HAS800t2 coating (a) Low and (b) high magnification

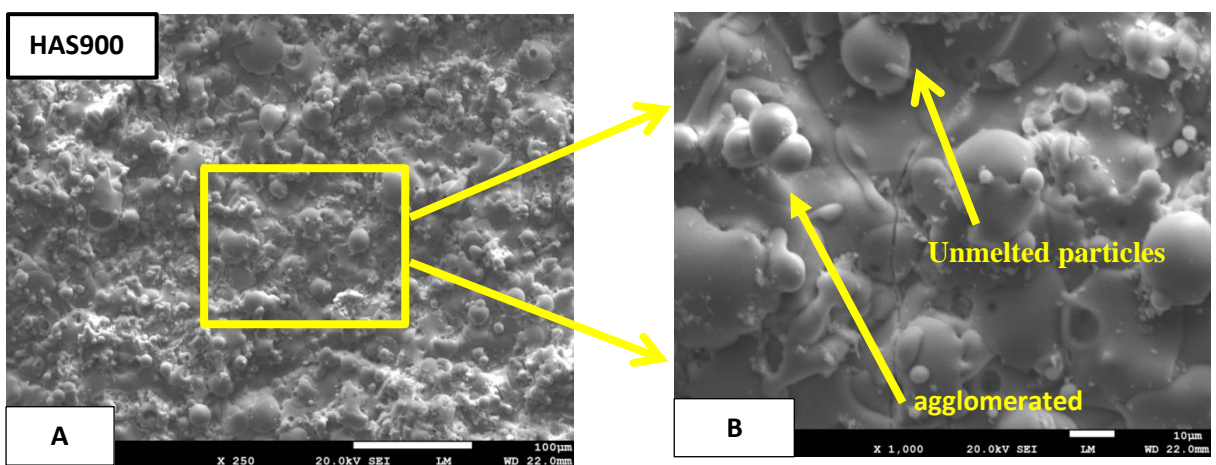


Fig. 4.8. FESEM micrographs of top HAS900t2 coating (a) Low and (b) high magnification

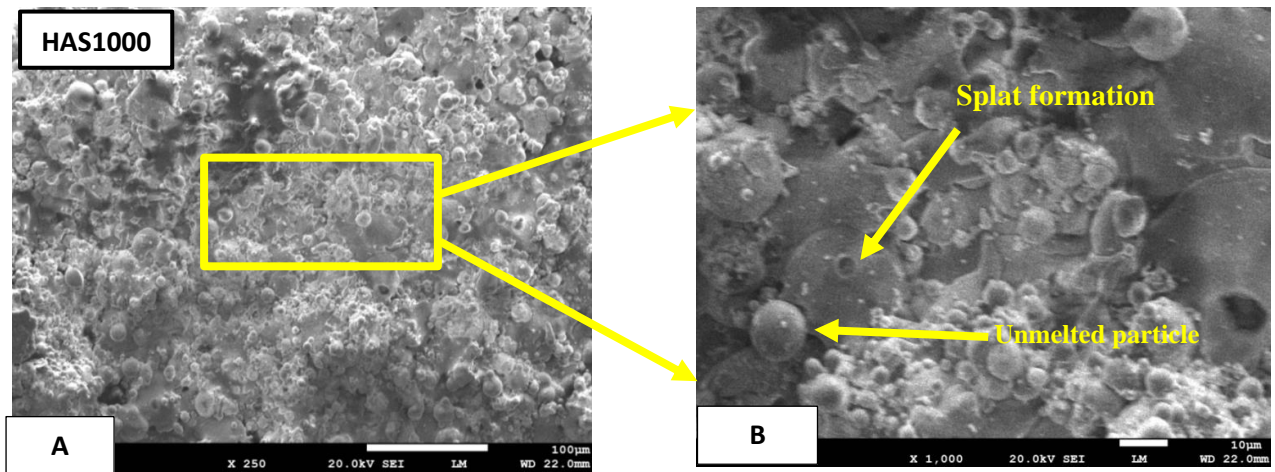


Fig. 4.9. FESEM micrographs of top HAS1000t2 coating (a) Low and (b) high magnification

4.5.2 Cross-section Morphology:

The internal (layer deposition) characteristics of coatings cannot be predicted from their surface morphology. As a result, field emission scanning electron microscopy is used to evaluate the polished cross-sections of the coated samples, as shown in Fig 4.10-4.14. The presence of a crystal lattice with cavitation at the coating-substrate interface has been identified. Inter-splat voids are observed in splats with very tiny diameters. Coated samples prepared from HA synthesized at 900 °C, and 1000 °C temperatures have fewer voids than the other coated samples depicted in Fig 4.13-4.14. A greater inter-particle boundary match results in increased bonding strength throughout the coating interface. More interlayer gaps can be found for HAS700t2 coating, as shown in Fig. 4.11. This is due to increased molten particle vaporization during spraying. Apart from the mechanical interlocking of the sprayed covering with the substrate, there may have been some metallurgical bonding at the interface, as clear by the existence of certain inter-diffusion zones as shown in Fig. 4.12, 4.13, and 4.14 for TCP, HAS700t2 and HAS800t2 coating, respectively.

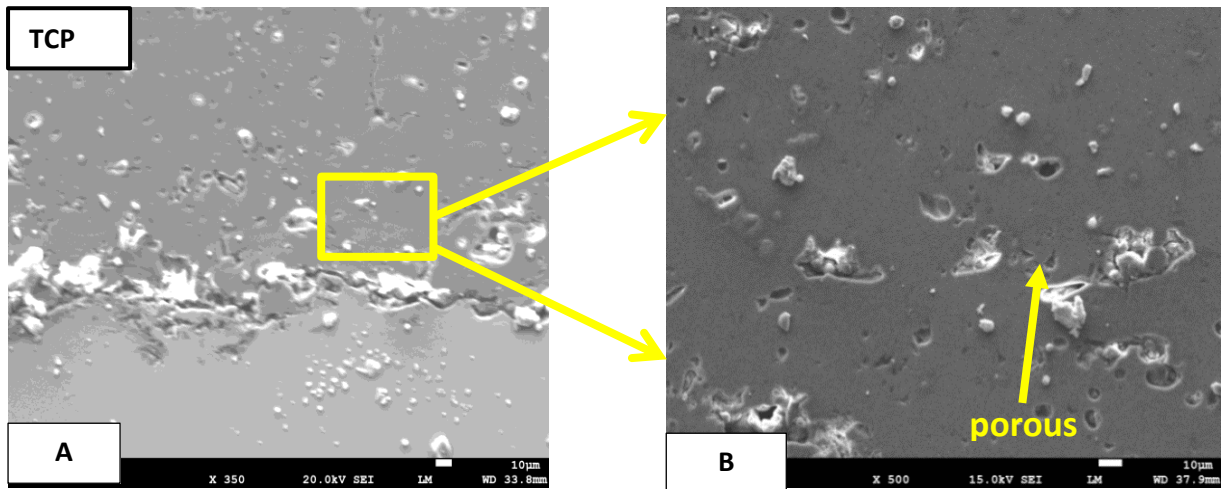


Fig. 4.10. FESEM micrographs of cross-section TCP coating (a) Low and (b) high magnification

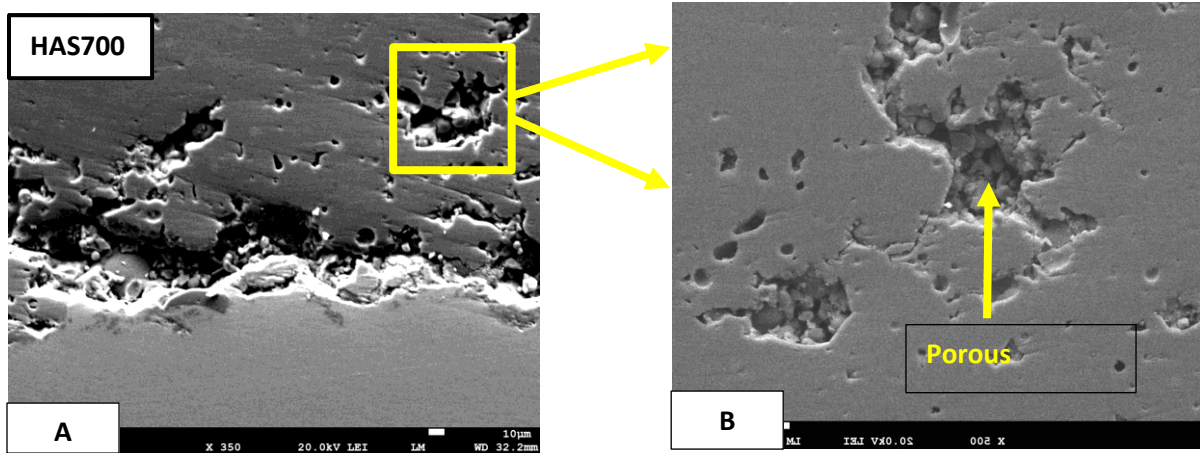


Fig. 4.11. FESEM micrographs of cross-section HAS700t2 coating (a) Low and (b) high magnification

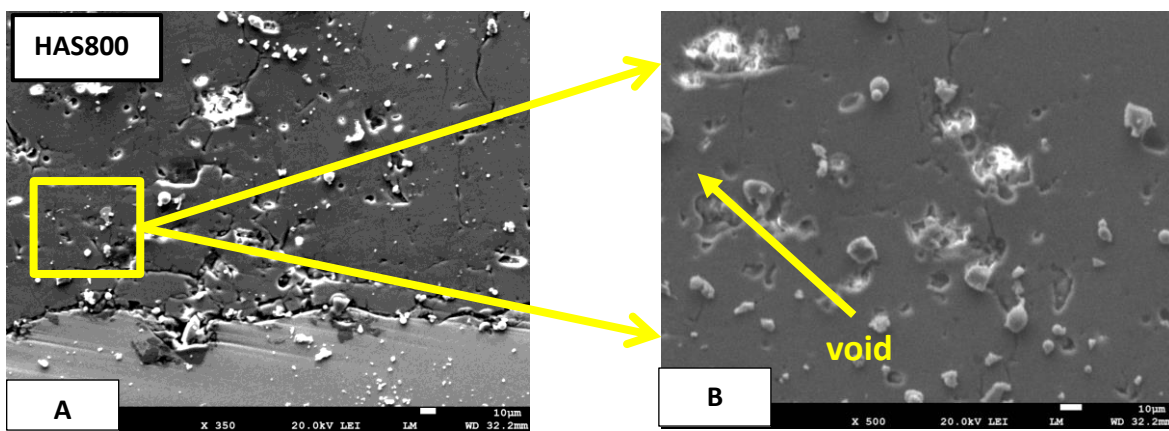


Fig. 4.12. FESEM micrographs of cross-section HAS800t2 coating (a) Low and (b) high magnification

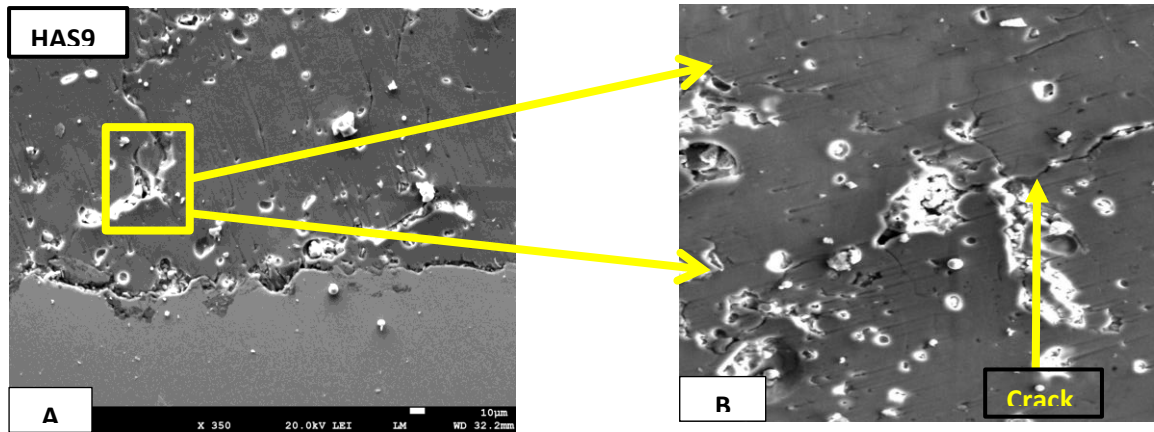


Fig. 4.13. FESEM micrographs of cross-section HAS900t2 coating (a) Low and (b) high magnification

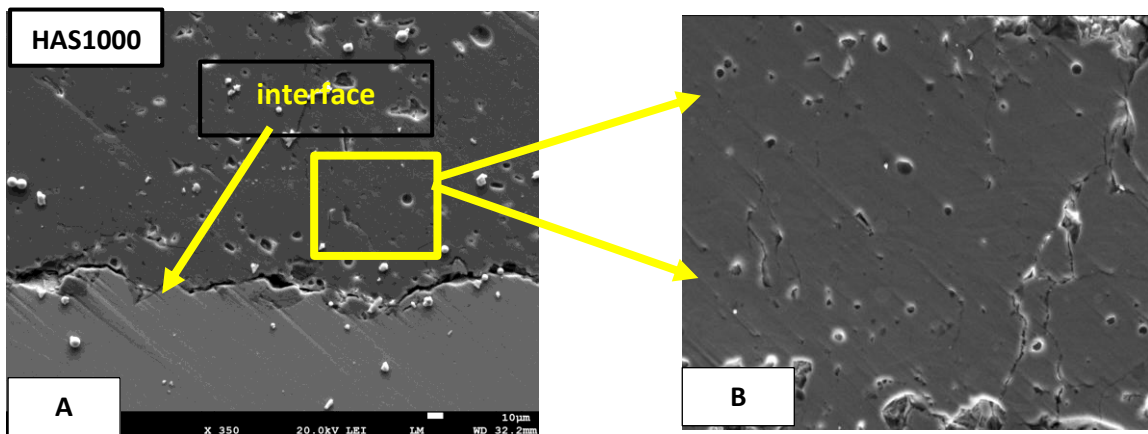


Fig. 4.14. FESEM micrographs of cross-section HAS1000t2 coating (a) Low and (b) high magnification

4.6 Microhardness Measurement:

Fig. 4.15 shows the representation of Vickers hardness value with increasing the synthesized temperature. It can be observed from Fig. 4.15 that when the synthesizing temperature rises, the coating hardness rises as well up to HAS900t2. This could be related to the formation/transformation of chemicals such as calcium and its oxides into allotropic forms, as well as compositional differences in the produced powder during spray deposition. If the synthesized temperature of powder is increased, then an increasing trend of hardness is observed due to the high rate of solidification, thermal conductivity, etc. Hardness is maximum at 900 °C because hydroxyapatite has a stable form at 900 °C. Hardness depends on the

composition of coatings as well as the phase of the coating. A high solidification rate tends to material become brittle, so hardness increases.

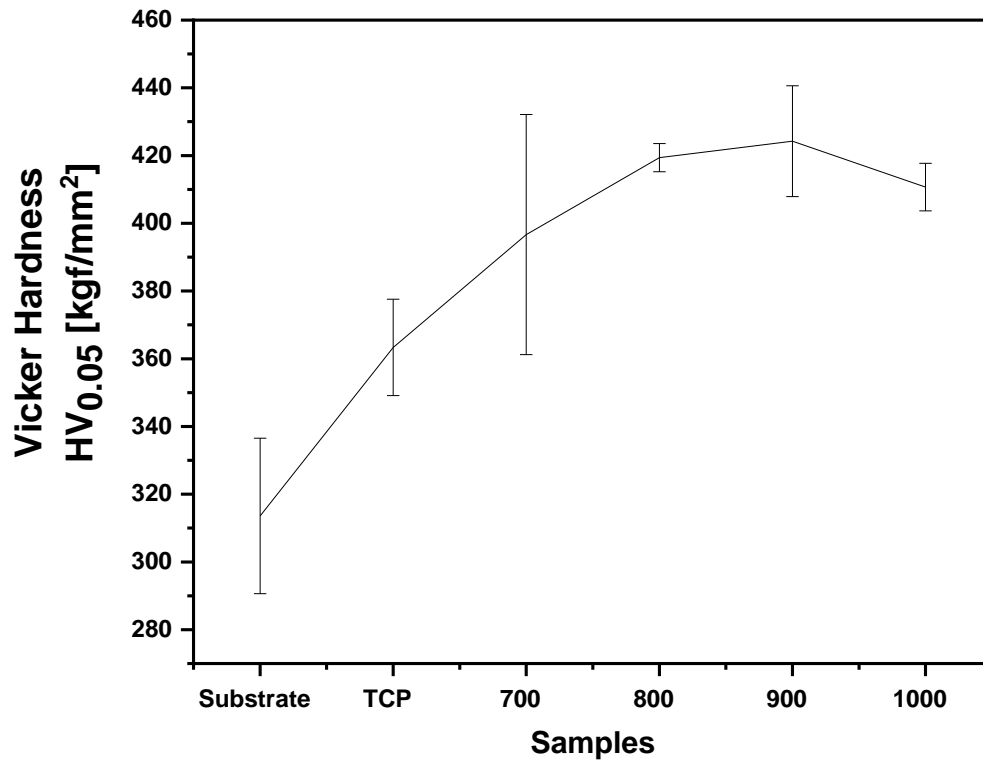


Fig. 4.15 Variation of Microhardness of TCP coating and various synthesized temperature

4.7 Scratch Analysis:

4.7.1. Scratch hardness and fracture toughness:

The scratch hardness and fracture toughness of the coatings are measured with a scratch testing machine using a constant load of 4 N. The variation of scratch hardness and fracture toughness follows a similar trend for all the five different coated samples, as shown in Fig. 4.16. Variation in the value of scratch hardness and fracture toughness is observed as the synthesis condition of HA powders changes. Scratch hardness is found to be maximum at 1000 °C, whereas a maximum value of fracture toughness is obtained at 800 °C as shown in Fig. 4.16. The scratch hardness of each coating decreased as the normal force increased, whereas the equivalent penetration depth increased in the other direction [24]. The toughness of coated sample varied in depth of penetration as a response to applied stress during the experimental period. As penetration depth significantly depends upon the material. The results of the XRD patterns

indicate that there is more amount of tricalcium phosphate present at a synthesized temperature of 800 °C, so significantly high scratch hardness and fracture toughness are observed at 800 °C. And further, it reduces at a synthesized temperature of 900 °C because hydroxyapatite has a stable phase at 900 °C, and there is more amount of calcium oxide will be present, which reduces scratch hardness and fracture toughness. Furthermore, scratch hardness and fracture toughness increase at 1000 °C because of the proper melting of the droplets, high solidification rate of melting droplets, and proper splat formation.

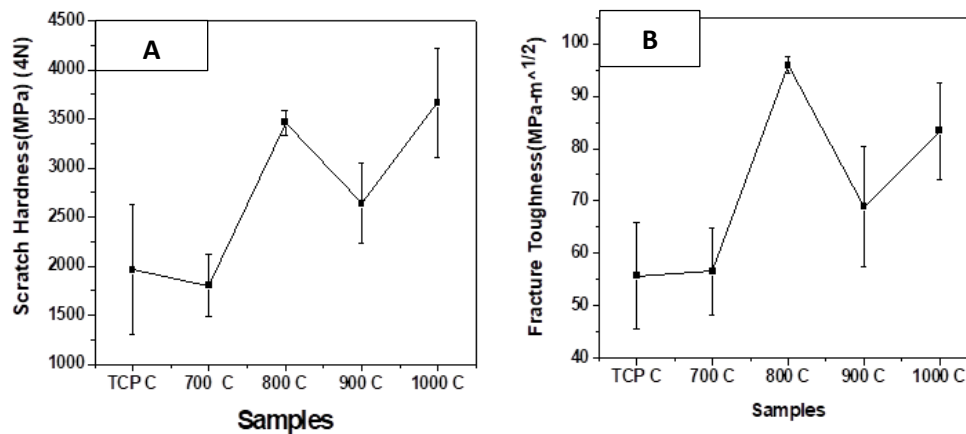


Fig. 4.16 Variation of (a) Scratch hardness and (b) Fracture Toughness of TCP coating and at various synthesized temperatures coatings at a load of 4 N

4.7.2. Coefficient of Friction and Tractional Force:

The variation of coefficient of friction and tractional force with respect to total length at a load of 4 N for five different coated samples are shown in Fig. 4.17-4.21. Variations in scratch friction coefficient (SFC) and frictional force over a scratch length were recorded while performing the tests at the coatings' top surface. In the initial stage, the scratch friction coefficient shows major fluctuations as the indenter experiences variable resistance at lower values of normal load. Fluctuations subsequently reduce with the rise in normal load, and values of scratch friction coefficient and frictional force increase steadily. Coatings with tougher reinforcement exhibit bigger variations. All coated specimens show a similar trend in frictional force measured across the length of the scratch. Under a scanning electron microscope, the morphological features of all scratch trails indicate no large-scale deformation. The material in front of the indenter will penetrate more into the coating so that the coating

material in front of the indenter is much more so that it will resist the indenter to propagate, and if the frictional force is too high, it will lead to the higher value of the coefficient of friction. Higher the value of the hardness of the coating, the penetration in the coating material is less. Thus, it will reduce the plugging component of friction, and a lesser value of the coefficient of friction is observed.

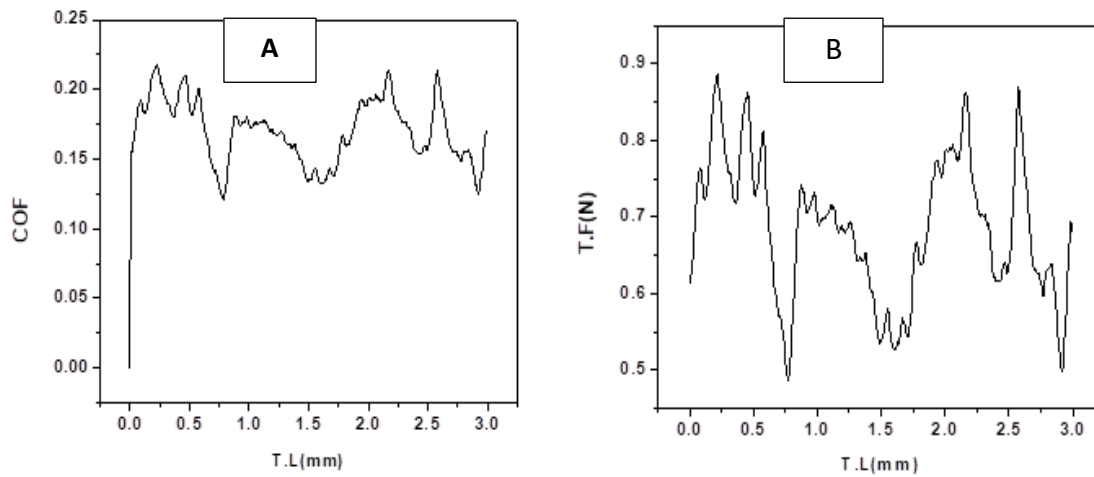


Fig. 4.17 (a) Variation of COF and (b) tractional force against travelling length at 4 N constant load for TCP coating

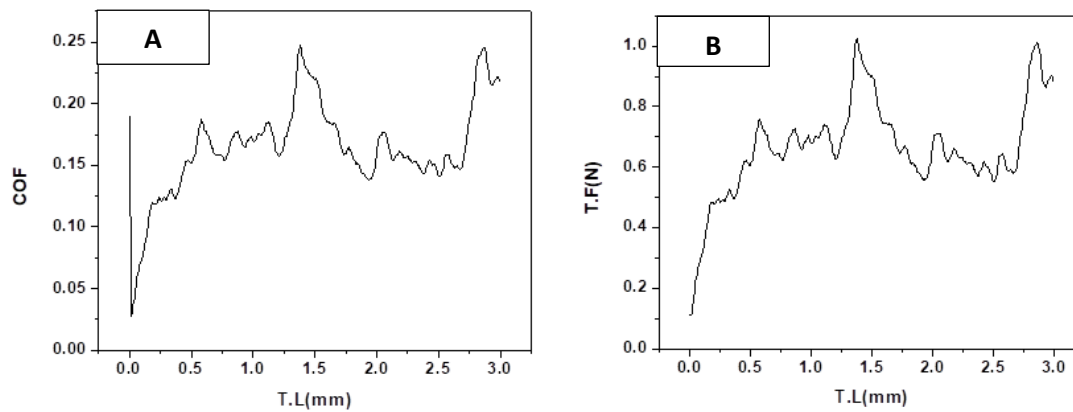


Fig. 4.18 (a) Variation of COF and (b) variation of tractional force against travelling length at 4 N constant load for HAS700t2 coating

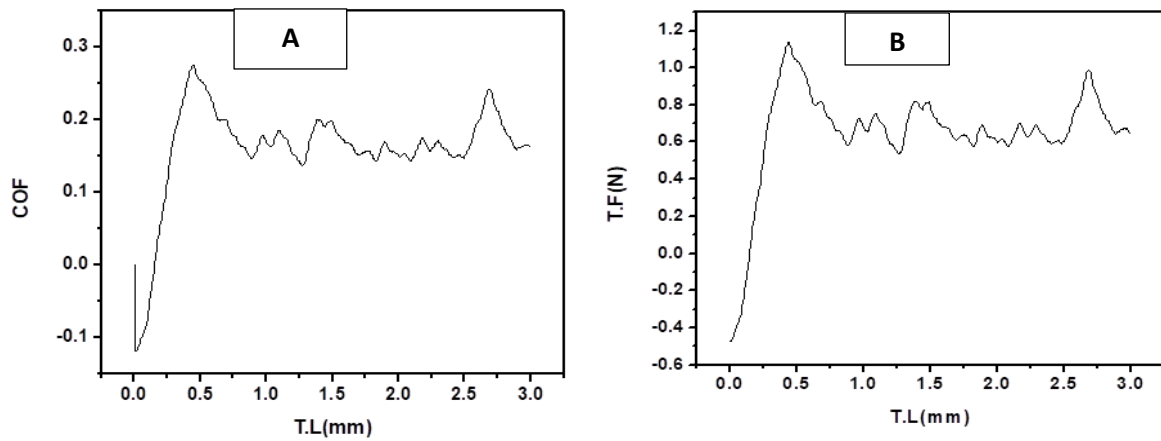


Fig.4.19 (a) Variation of COF and (b) variation of tractional force against travelling length at 4 N constant load for HAS800t2 coating

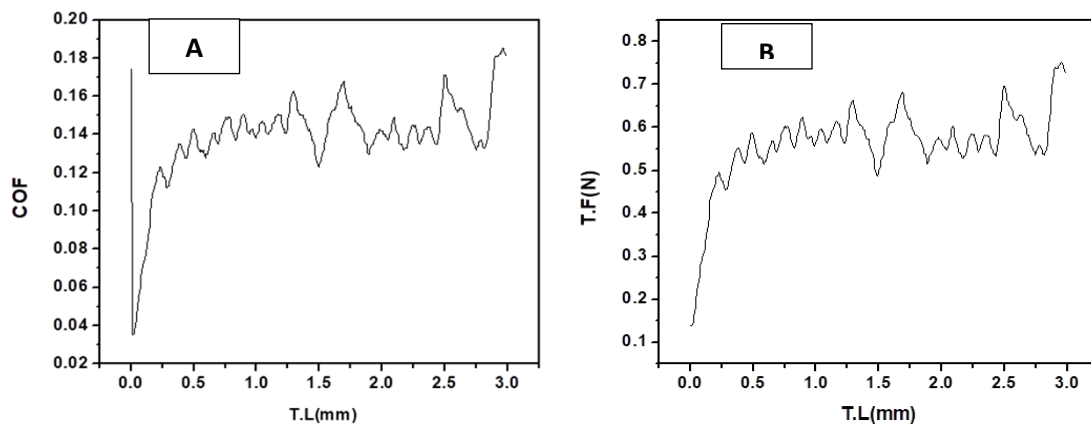


Fig.4.20 (a) Variation of COF and (b) Variation of tractional force against travelling length at 4 N constant load for HAS900t2 coating

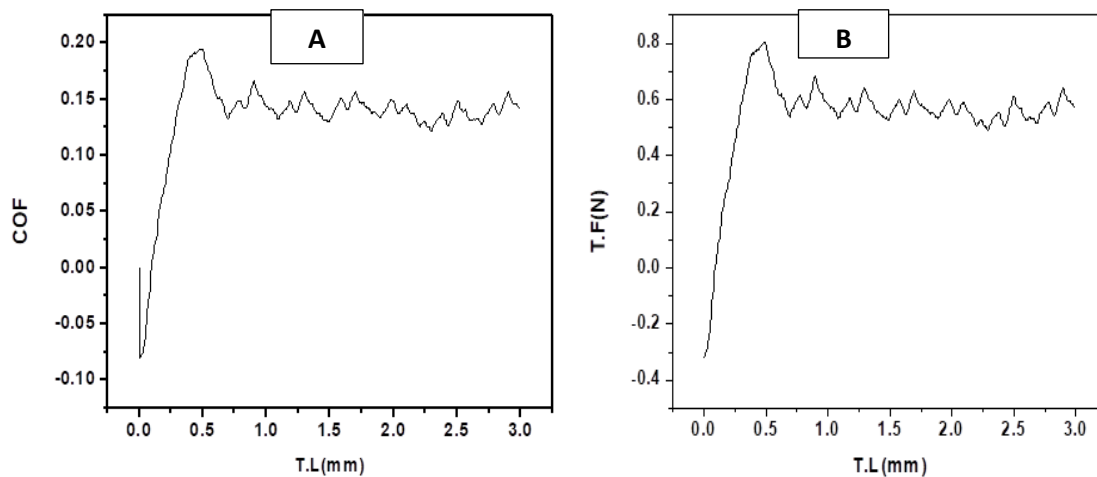


Fig. 4.21 (a) Variation of COF and (b) Variation of tractional force against travelling length at 4 N constant load for HAS1000t2 coating

4.8 Wear Analysis:

The specific wear rate values of five different coatings are as shown in Fig. 4.22. When the coating is changed from TCP to HA800t2, the specific wear rate is found to be increased gradually. Further increase in synthesis temperature of HA at 900 leads to a decrease in the specific wear rate of the coating. The maximum value of the specific wear rate is obtained for the HAS1000t2 coated sample. This is because, at 1000 °C synthesized temperature, the coating will show a higher resistance to plastic deformation due to wear. So, it will reduce the formation of debris at the wear track. The lesser extent of damage leads to the lower value of the specific wear rate.

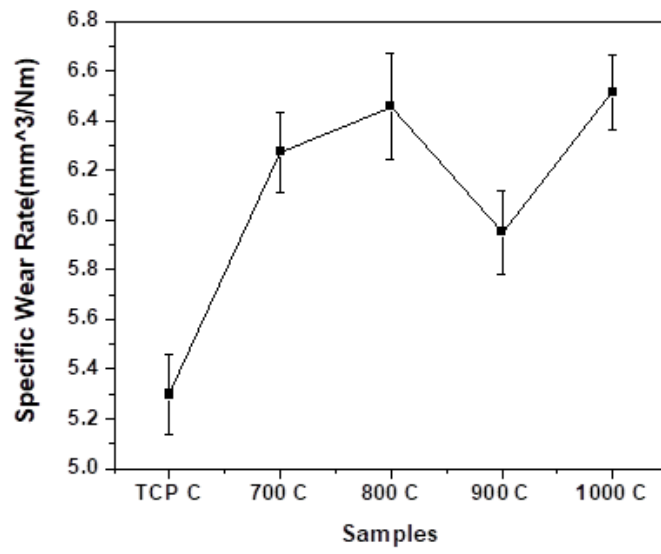


Fig. 4.22. Value of specific wear rate of TCP coating and at various synthesized temperature coatings

Chapter 5

Conclusions

1. Among the five coatings, the defects are maximum in the HAS700t2 sample. Hence, the roughness of the coating is the maximum. On the other hand, defects in the HAS1000t2 sample are the minimum, and the melting of such coating is good, which leads to developing HA coating with minimum roughness.
2. The formation of CaO is more in the HAS900t2 sample compared to the other coatings. This gives the coating some extra hardness and makes it the hardest among all coatings. However, during the wear test, such CaO forms Ca (OH)₂ by adsorbing H₂O from the atmosphere and reducing the wear resistance of the coating. On the other hand, having the highest HA and TCP phases, the HAS1000t2 sample possesses the highest wear resistance property.
3. Excellent melting behavior of HAS1000t2 and HAS800t2 powders leads to the form HA coatings with low porosity. Apart from that, the presence of TCP and HA phases in such coatings has helped to improve the toughness of HAS1000t2 and HAS800t2 coatings.
4. All the five coatings are found to strongly adhere to Ti-alloy substrates. Even at 20 N of normal load the coatings are found to be intact, and no failure has occurred. HAS900t2 and HAS1000t2 coatings possibly possess potential coating characteristics such as good adhesion strength, hardness, porosity, etc.
5. The XRD graph shows that the stable phase and almost pure hydroxyapatite are obtained at 1000 °C synthesized temperature. The microstructure of the coatings is also dependent on the physical characteristics such as porosity and phase transformations of the coating materials.
6. The roughness of the coating is first increased and then decreases as the synthesized temperature rises. It has been noticed as the synthesizing temperature is raised from 700 °C to 900 °C, the coating hardness increases, and further increments in temperature lead to decreases in the hardness.

References

- [1] American Society of Materials. "Introduction to Thermal Spray Processing," Handbook of Thermal Spray Technology, ASM International, Cleveland, Ohio.
- [2] **Andrew J. Ruys, Brett A. Sutton, 2021.** in Metal-Reinforced Ceramics,
- [3] **Guohong wang,** Surface and Coatings Technology Volume 367, 15 June 2019, Pages 225-230 ,Effect of post-heat treatment on the microstructure of micro-plasma sprayed hydroxyapatite coatings,
- [4] **Roumnik unabia** Journal of the European Ceramic Society Volume 39, Issue 14, November 2019, Pages 4255-4263, Investigation on the structural and microstructural properties of copper-doped hydroxyapatite coatings deposited using solution precursor plasma spraying,
- [5] **Heimann, B.,** 1996, ISBN 3-527-29430-9 Plasma Spray Coating, VCH Publishers, New York, Chapter 3.
- [6] **Harjeet Singh et al.** Volume 50, Part 5, 2022, Pages 612-628 HA-based coating by plasma spray techniques on titanium alloy for orthopedic applications
- [7] **M. P. Taylor,** "Assessment of plasma-sprayed hydroxyapatite coatings", PhD Thesis, University of Birmingham, Birmingham, 1994.
- [8] **J. Tanya, BEng Levingstone,** Journal of the Mechanical Behavior of Biomedical Materials Volume 101, January 2020, 103418 Dublin City University, Ireland, 2000"Optimization of Plasma Sprayed Hydroxyapatite Coatings" School of Mechanical and Manufacturing Engineering,

[9] **Jia Ren, Dong Zhao**, 2020 Journal of the Mechanical Behavior of Biomedical Materials Volume 101, January 2020, 103418 ,Heat and hydrothermal treatments on the microstructure evolution and mechanical properties of plasma sprayed hydroxyapatite coatings.

[10] **P. Fauchais**, ", vol. 37, pp. R86, 2004, Journal of Physics D: Applied Physics.
"Understanding plasma spraying

[11] **Y. Yang and E. Chang**, " Surface and Coatings Technology, vol.190, pp. 122-131, 1/3. 2005 "Measurements of residual stresses in plasma sprayed Hydroxyapatite coatings on titanium alloy

[12] **R McPherson**. Vol. 39, No. 40, 173-181, 1989“A Review of Microstructure and Properties of Plasma Sprayed Ceramic Coatings”, Surface and Coatings Technology,

[13] **H.W. Ng, Z. Gan**,” Finite Elements in Analysis and Design 41, 1235-1254, 2005]
“A finite element analysis technique for predicting as-sprayed Residual stresses generated by the plasma spray coating process

[14] **Saed Safai, Herbert Herman**”, Thin Solid Films, Vol. 45, 295-307, 1977
“Microstructural Investigation of Plasma Sprayed Aluminum Coatings

[15] **N Venkatramani**, Current Science, Vol 83, No. 3, 254-262, 2002. “Industrial plasma torches and applications”,

[16] **Amirhossein Goharian**, 2017, March 2017 Elsevier ISBN: 978012804634, Mohamed R. Abdullah, in Trauma Plating Systems

[17] **S.M. Muneer**, 2018 Volume 5, Issue 11, Part 3, 2018, Pages 23834-23843, Wear characterization and microstructure evaluation of silicon carbide-based Nano composite Coating using plasma spraying,

[18] **Zhang, S.**, 2013, 10.1201/b14803 Boca Raton, USA: CRC Press Hydroxyapatite Coatings for Biomedical Applications: Advances in Materials Science and Engineering.

[19] **Ronaldo candidato, 2017** Surface and Coatings Technology Volume 318, 25 May 2017, Pages 39-49, Development of hydroxyapatite coatings by solution precursor plasma spray process and their microstructural characterization,

[20] **De Groot, K., R. Geesink, C.P. Klein, and P. Serekian**, 1987. 21(12): p. 1375-1381 Plasma sprayed coatings of hydroxyapatites. Journal of Biomedical Materials Research.

[21] **Kazi Sabiruddin, Shahid Hussain**. Ceramics International, Volume 47, Issue 21, 1 November 2021, Pages 29660-29669, The effect of heat treatments on the hydrothermal technique of hydroxyapatite production from Indian clam seashell.

[22] **Ramazan Sobhanverdi, Alireza Akbari**. Ceramics International, Volume 41, Issue 10, Part B, December 2015, Pages 14517-14528, Porosity and microstructural features of plasma sprayed Ytria stabilized Zirconia thermal barrier coatings.

[23] **Ctibor P.** et al. Vol. 262, 1274-1280, 2007 “Plasma Sprayed Ceramic Coatings without and with Epoxy Resin Sealing Treatment and Their Wear Resistance”

[24] **Vaibhav Nemane, Satyajit Chatterjee**. Materials Characterization, Volume 180, October 2021, 111414, Evaluation of microstructural, mechanical, and tribological characteristics of Ni-B-W-Sic electroless composite coatings involving multiphases scratch test.

[25] <https://researchbank.swinburne.edu.au>